Diboson resonance and vector-like quark searches at ATLAS and CMS

Miaoran Lu

On behalf of the ATLAS and CMS collaboration

29/5/2020

Outline

Focus only on recent results from ATLAS & CMS

Diboson resonance:

1. ATLAS: $X \to VH \to qq\, b\bar{b}$ (just approved)
2. CMS: $X \to VV \to qq\, qq$ (arXiv:1906.05977)
3. ATLAS: $qq(VBF) \to HH\, qq \to b\bar{b}\, b\bar{b}\, qq$ (arXiv:2001.05178)
4. CMS: $X \to HH \to b\bar{b}\, WW \to b\bar{b}\, qq'\, \ell\nu$ (arXiv:1904.04193)
5. ATLAS: $X \to VV \to V_\ell V_h$(semi-leptonic) (arXiv:2004.14636)
6. ATLAS: $A \to BC \to JJ$ (arXiv:2005.02983)

Vector-like quarks:

1. ATLAS: $qg \to Y(T)\, q'\bar{b} \to Wb\, q'\bar{b} \to l\nu b\, q'\bar{b}$ (arXiv:1812.07343)
2. ATLAS: $qg \to T\, q'\bar{b} \to Zt\, q'\bar{b} \to \bar{\nu}\nu\, bq\bar{q}'\, q'\bar{b}$ (arXiv:1812.09743)
3. CMS:

   $qg \to T\, q'\bar{b} \to Ht\, q'\bar{b} \to b\bar{b}t\, q'\bar{b}$,
   $qg \to T\, q'\bar{b} \to Zt\, q'\bar{b} \to b\bar{b}t\, q'\bar{b}$,
   $qg \to T\, q\bar{t} \to Ht\, q\bar{t} \to b\bar{b}t\, q\bar{t}$,
   $qg \to T\, q\bar{t} \to Zt\, q\bar{t} \to b\bar{b}t\, q\bar{t}$,
   (arXiv:1909.04721)

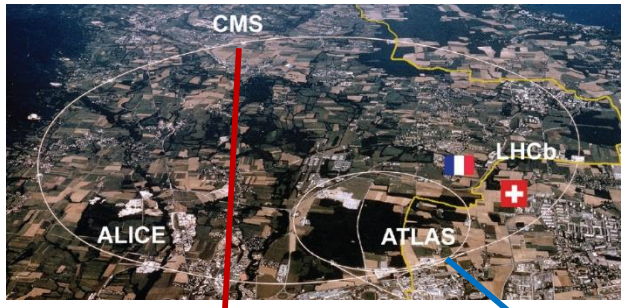

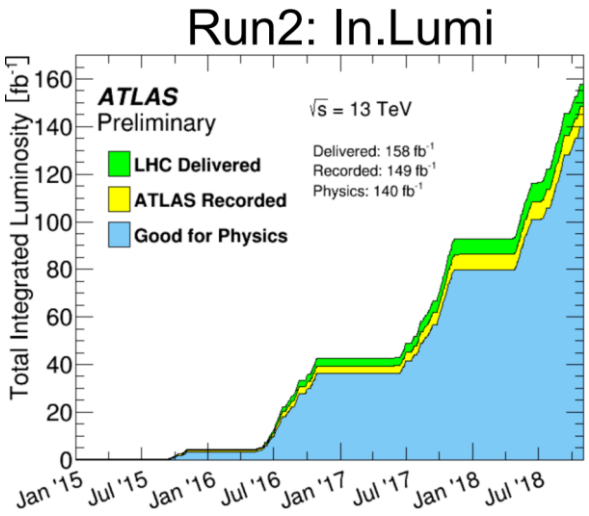

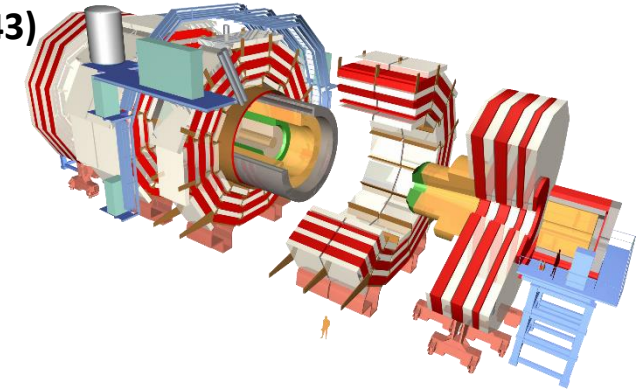

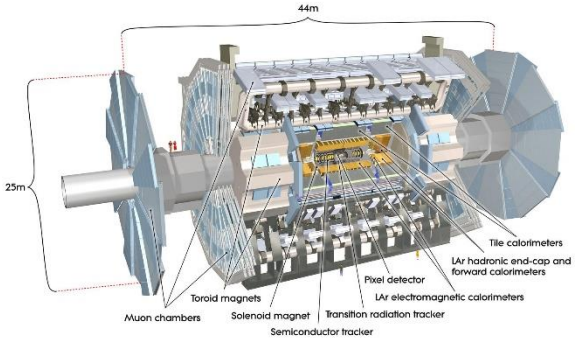

Diboson resonance search

SM shortcomings indicate some kind of **New Physics**
(Hierarchy problem, Unific.of Gravity, Dark Matter/Energy)

Many BSM theories have been proposed:
(Extended Gauge-Symmetry models; RS Warped ED;
Two Higgs doublet models; Little/Composite Higgs)

Predicting new heavy boson(s) X :
spin-0 : Radion
spin-1 : HVT Z', W'
spin-2 : Kaluza–Klein graviton (GKK)

at the TeV scale decaying to a pair of SM boson(W, Z, H, γ)

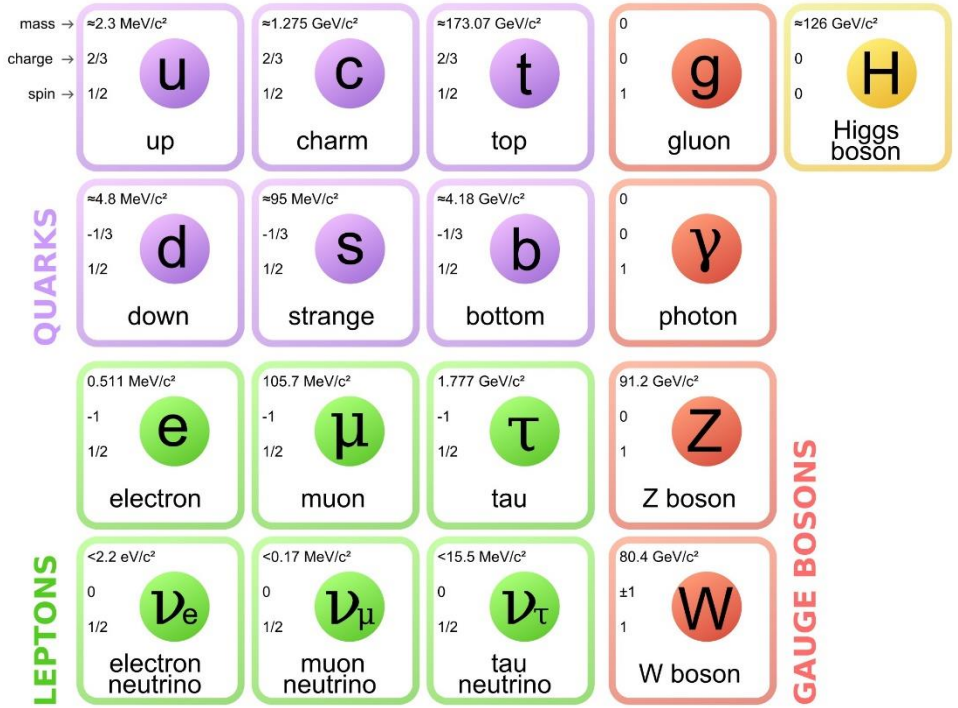

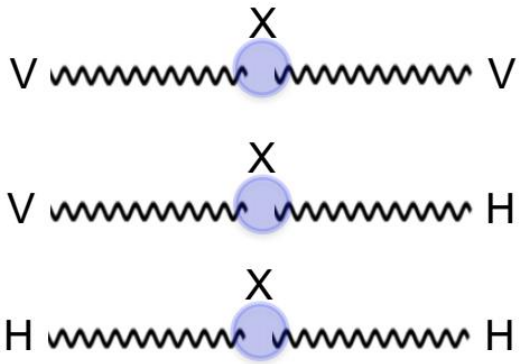

Search for VH resonances in hadronic final states ATLAS

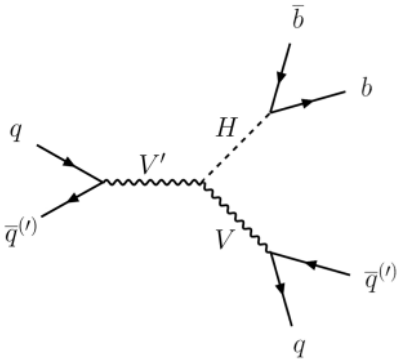

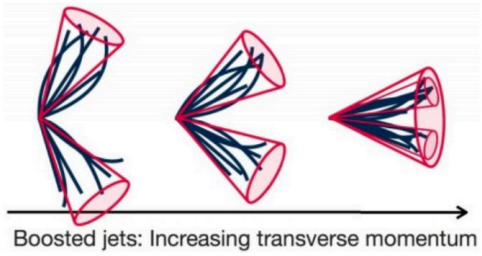

Signal model:

spin-1 : Z', W', HVT Model A and B

Main background: multijet

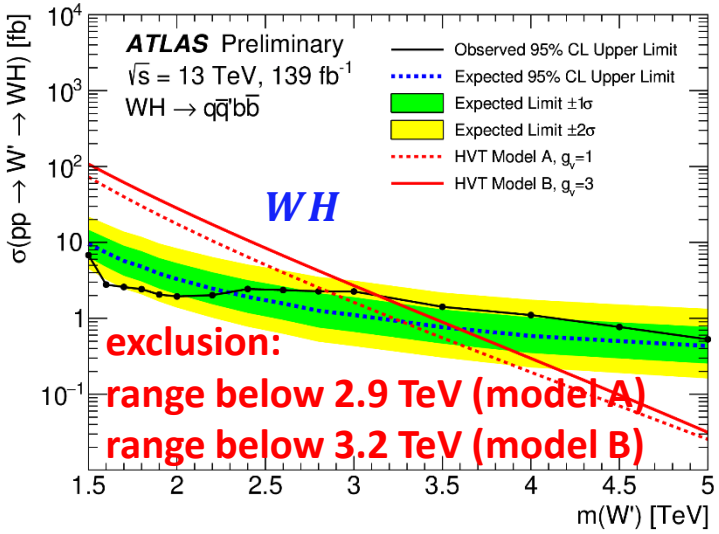

exclusion:

range below 2.9 TeV (model A)

range below 3.2 TeV (model B)

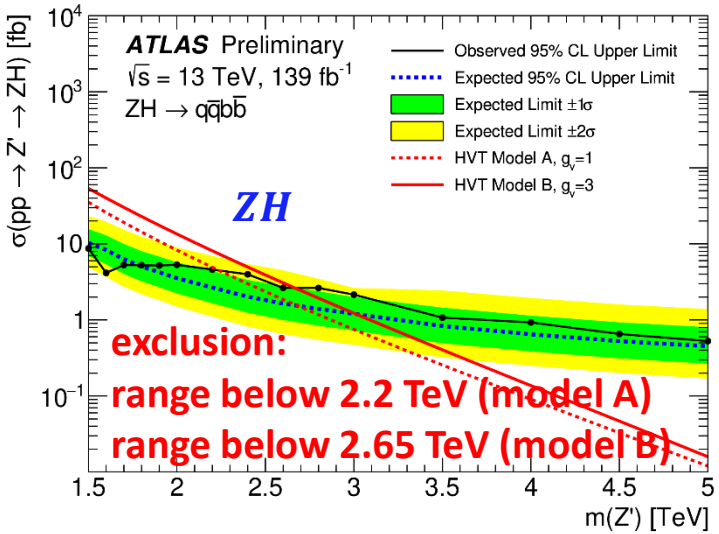

exclusion:

range below 2.2 TeV (model A)

range below 2.65 TeV (model B)

Preselection	Veto non-$qqqq$ channels: No e (μ) with $p_T > 7$ GeV and $\|\eta\| < 2.47$ (2.5) Event kinematics: ≥ 2 large-R jets with $p_T > 200$ GeV and $\|\eta\| < 2.0$ leading large-R jet with $p_T > 500$ GeV leading and subleading large-R jets with $m_{JJ} > 1.3$ TeV leading and subleading large-R jets with $\|\Delta y\| < 1.6$
Signal region (SRWH / SRZH)	V and H bosons: V-boson (H-boson) candidate is large-R jet with lower (higher) mass W-boson candidate with W jet mass window, D_2, and n_{trk} Z-boson candidate with Z jet mass window, D_2, and n_{trk} H-boson candidate with H jet mass window and n_{trk}, 1 or 2 b-tagged track jets

***W* and *Z* highly boosted, reconstructed as single large R jet**

Use jet substructure information to tag signal jets

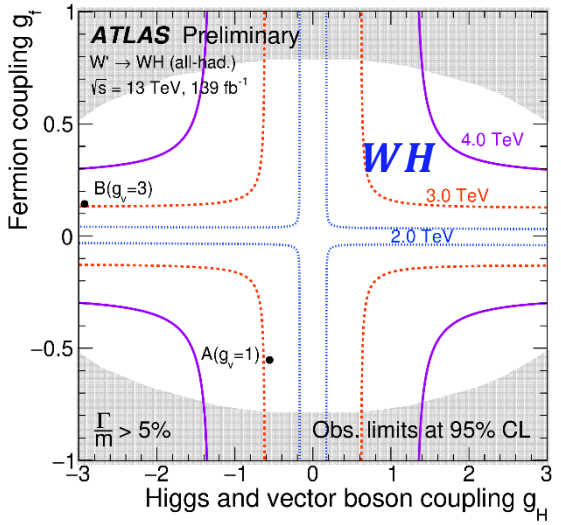

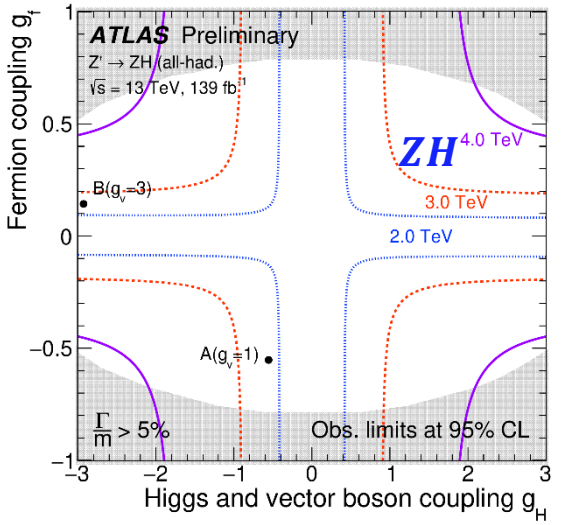

g_f, g_q, g_H: coupling strength of V' to fermions, quarks, and Higgs (g_q is taken to be equal to g_f)

multi-dimensional search for diboson resonances in the dijet final state CMS

X → VV → qq qq

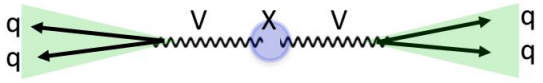

Signal model:

1. **spin-1 : Z', W', HVT Model B**
2. **spin-2 : Kaluza–Klein graviton (GKK), bulk RS model**

Signature:

1. **large R jet**
2. **"groomed" jet mass**
3. **N-subjettiness ratio $\tau_{21} = \tau_2/\tau_1$**

Main background: multijet

Category	HPHP	HPLP
W+jets	100 ± 11	4600 ± 200
Z+jets	33 ± 4	1580 ± 160
QCD multijets	650 ± 4	51100 ± 300
Predicted total background	783 ± 12	57200 ± 400
Observed yield	780 ± 30	57230 ± 240

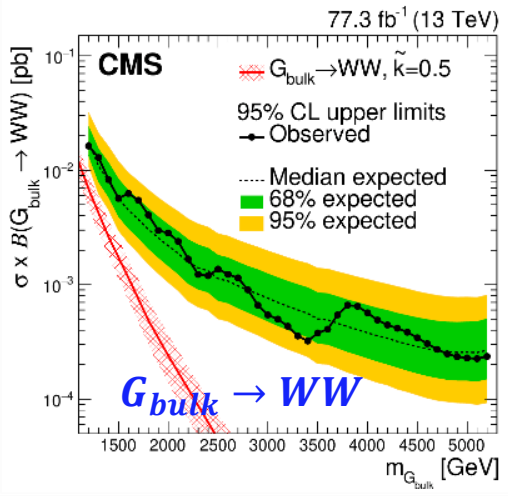

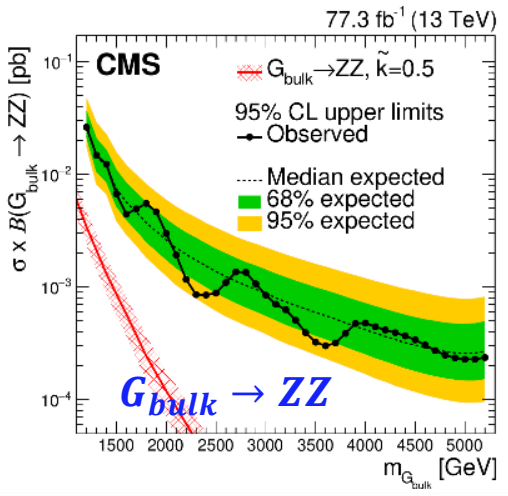

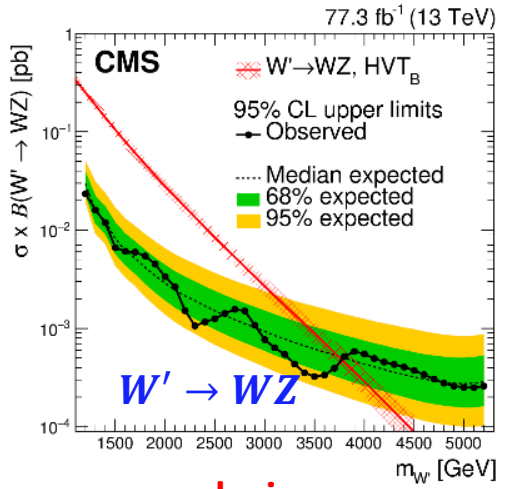

exclusion: range below 3.8 TeV

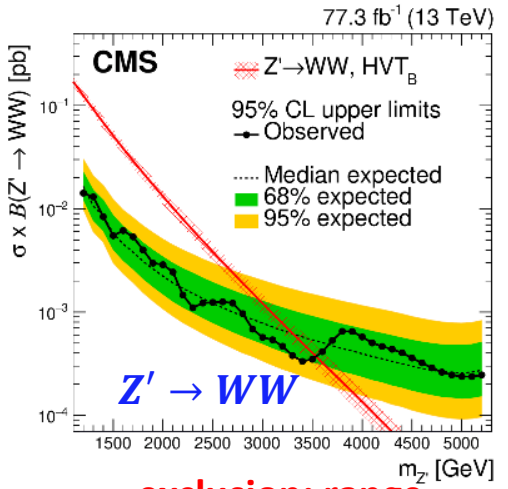

exclusion: range below 3.5 TeV

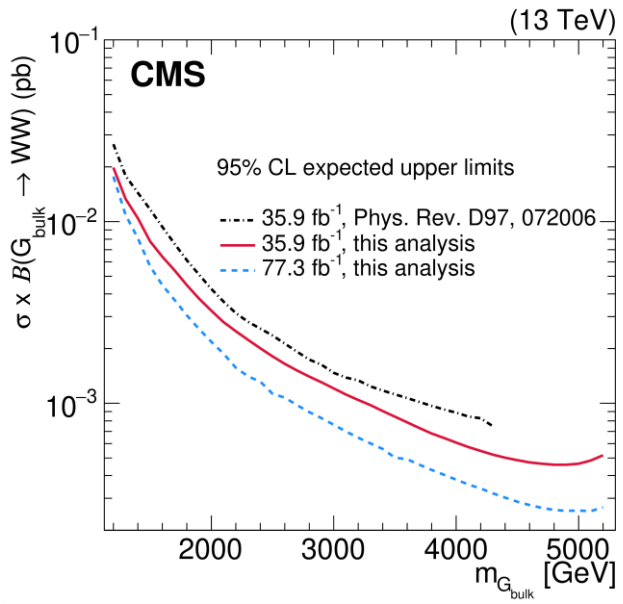

Improvement in sensitivity of up to 30% relative to previous search methods with three-dimensional (M_{J1}, M_{J2}, M_{JJ}) maximum likelihood fit

https://arxiv.org/abs/1906.05977, Eur. Phys. J. C 80 (2020) 237

$HH \to b\bar{b}b\bar{b}$ VBF production ATLAS

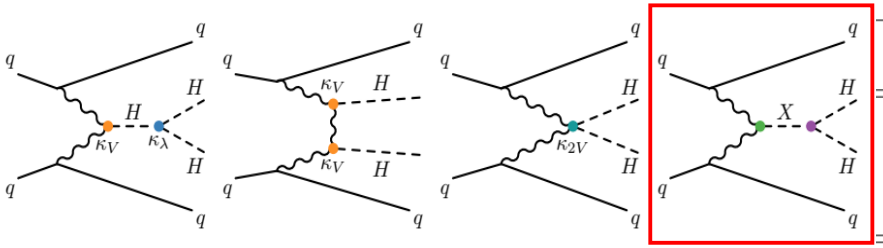

Two classes of signals:

1. a **broad resonance** with width 10-20% of the signal mass
2. a **narrow resonance** with a fixed width of 4 MeV

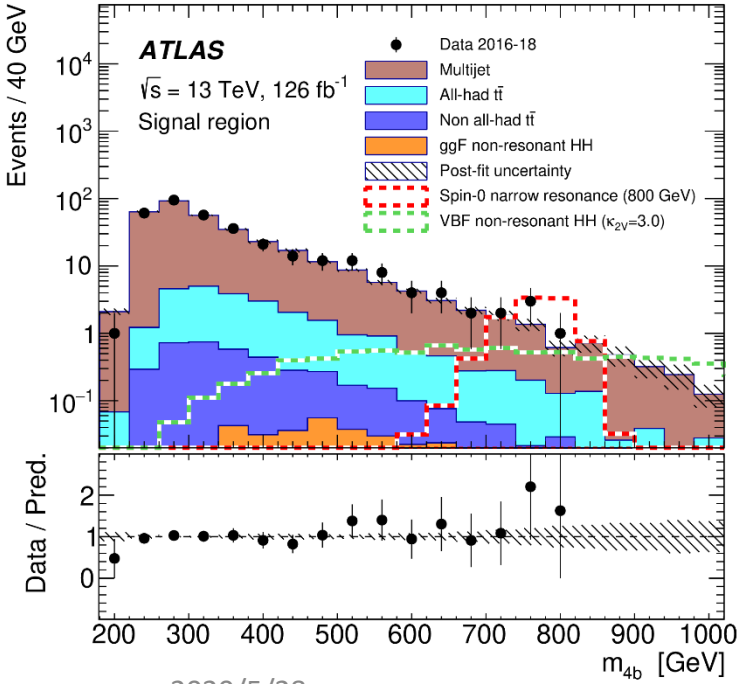

Selections	
At least two jets with $p_T > 30$, $\lvert\eta\rvert > 2.0$	Two highest-p_T jets with opposite sign η
	$\lvert\Delta\eta_{jj}^{VBF}\rvert > 5.0$ and $m_{jj}^{VBF} > 1000$
Exactly 4 b-tagged jets with $p_T > 40$, $\lvert\eta\rvert < 2.0$	
If $m_{4b} < 1250$	$\frac{360}{m_{4b}} - 0.5 < \Delta R_{bb}^{lead} < \frac{653}{m_{4b}} + 0.475$
	$\frac{235}{m_{4b}} < \Delta R_{bb}^{subl} < \frac{875}{m_{4b}} + 0.35$
If $m_{4b} \geq 1250$	$\Delta R_{bb}^{lead} < 1$
	$\Delta R_{bb}^{subl} < 1$
Pairs with minimum $D_{HH} = \sqrt{(m_{2b}^{lead})^2 + (m_{2b}^{subl})^2}\left\lvert\sin\left(\tan^{-1}\left(\frac{m_{2b}^{subl}}{m_{2b}^{lead}}\right) - \tan^{-1}\left(\frac{116.5}{123.7}\right)\right)\right\rvert$	
	$\lvert\Delta\eta_{HH}\rvert < 1.5$
Multijet	$\lvert\Sigma_i \vec{p}_{T,i}\rvert < 60$, where i = b-jets and VBF-jets
	$p_{T,H}^{lead} > 0.5 m_{4b} - 103$
	$p_{T,H}^{subl} > 0.33 m_{4b} - 73$
$t\bar{t}$	Veto if $X_{Wt} = \sqrt{\left(\frac{m_W - 80.4}{0.1 m_W}\right)^2 + \left(\frac{m_t - 172.5}{0.1 m_t}\right)^2} \leq 1.5$
Signal region (SR)	$X_{HH} = \sqrt{\left(\frac{m_{2b}^{lead} - 123.7}{11.6}\right)^2 + \left(\frac{m_{2b}^{subl} - 116.5}{18.1}\right)^2} < 1.6$

VBF topology

Higgs pair assignment

Main background: multijet and $t\bar{t}$

Background rejection

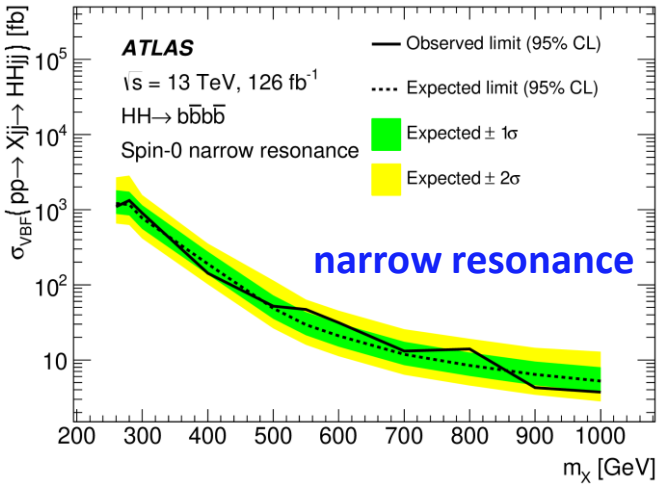

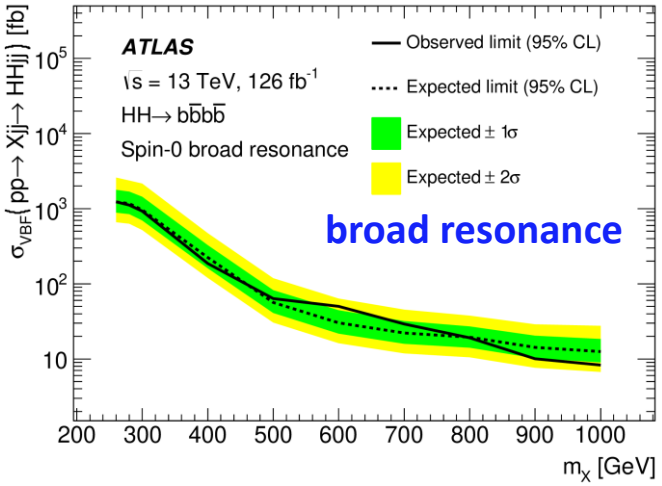

https://arxiv.org/abs/2001.05178, Submitted to JHEP

Heavy resonance decaying to HH in $b\bar{b}q\bar{q}'l\nu$ final states CMS

X → HH → bbWW* → bbqqlv

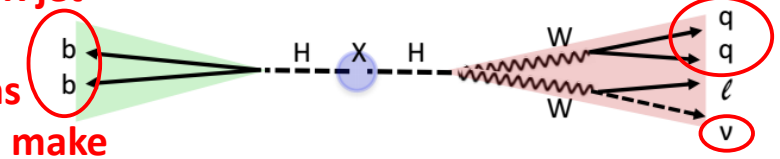

One large R jet (bb jet), corrections applied to make $\langle M_{bb} \rangle$ = 125 GeV

One large R jet (qq jet)

p_z of the neutrino estimated by setting the invariant mass of the neutrino, the lepton, and the qq' jet to m_H and solving the corresponding second-order equation

Categorization type	Selection	Category label
Lepton flavor	Electron	e
	Muon	μ
$b\bar{b}$ jet subjet b tagging	One medium	bL
	One medium and one loose	bM
	Two medium	bT
$q\bar{q}'$ jet substructure	$0.55 < q\bar{q}'\ \tau_2/\tau_1 < 0.75$	LP
	$q\bar{q}'\ \tau_2/\tau_1 < 0.55$	HP

Simultaneously estimating the signal and background yields using a maximum likelihood fit to the data in the 12 event categories and in the plane of the bb jet mass and the HH resonance mass

Signal model:

1. spin-0 : Radion, Randall–Sundrum framework
2. spin-2 : Kaluza–Klein graviton (GKK), bulk RS model

Signature:

1. Presence of bb jet and qq jet
2. Back-to back: $\Delta R(l, qq) < 1.2$, $\Delta\varphi(\ell, bb) > 2$, $\Delta R(bb, qq) > 1.6$

Main background: $t\bar{t}$, multijet, and W+jets

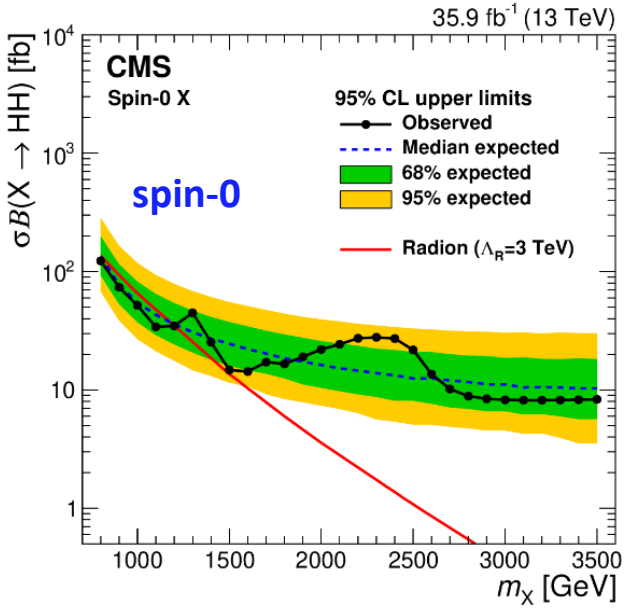

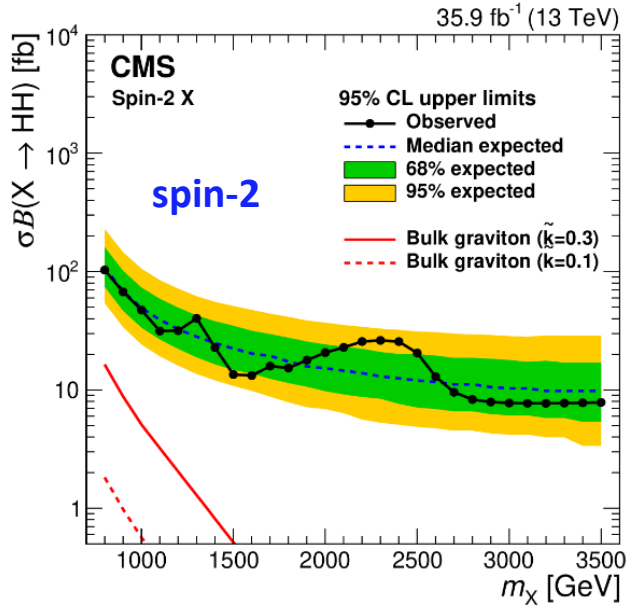

First result from CMS in this decay channel

https://arxiv.org/abs/1904.04193, JHEP 10 (2019) 125

Search for heavy diboson resonances in semi-leptonic final states ATLAS

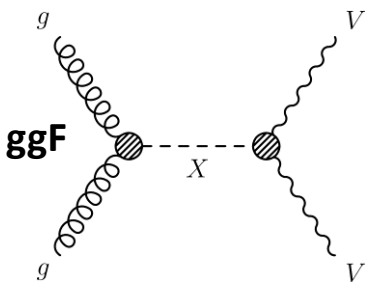

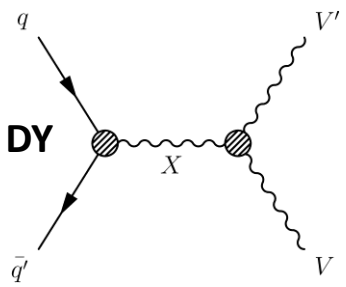

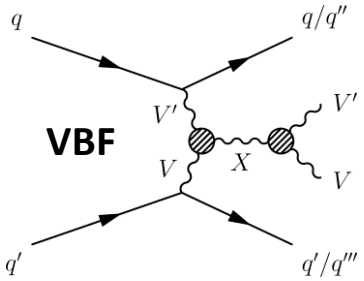

Signal model:

1. spin-0 : Radion, Randall–Sundrum framework
2. spin-1 : Z', W', HVT Model A, B, and C
3. spin-2 : Kaluza–Klein graviton (GKK), bulk RS model

Main backgrounds:

0 lepton: Z+jets and W+jets

1 lepton: W+jets and $t\bar{t}$

2 lepton: Z+jets

Final discriminants:

0 lepton: m_T

1 lepton: $m_{\ell\nu J}$ or $m_{\ell\nu jj}$

2 lepton: $m_{\ell\ell J}$ or $m_{\ell\ell jj}$

0 lepton: $Z \to \nu\nu$
1 lepton: $W \to \ell\nu$
2 lepton: $Z \to \ell\ell$

$X \to VV \to V_\ell V_h$ selection flow schematic

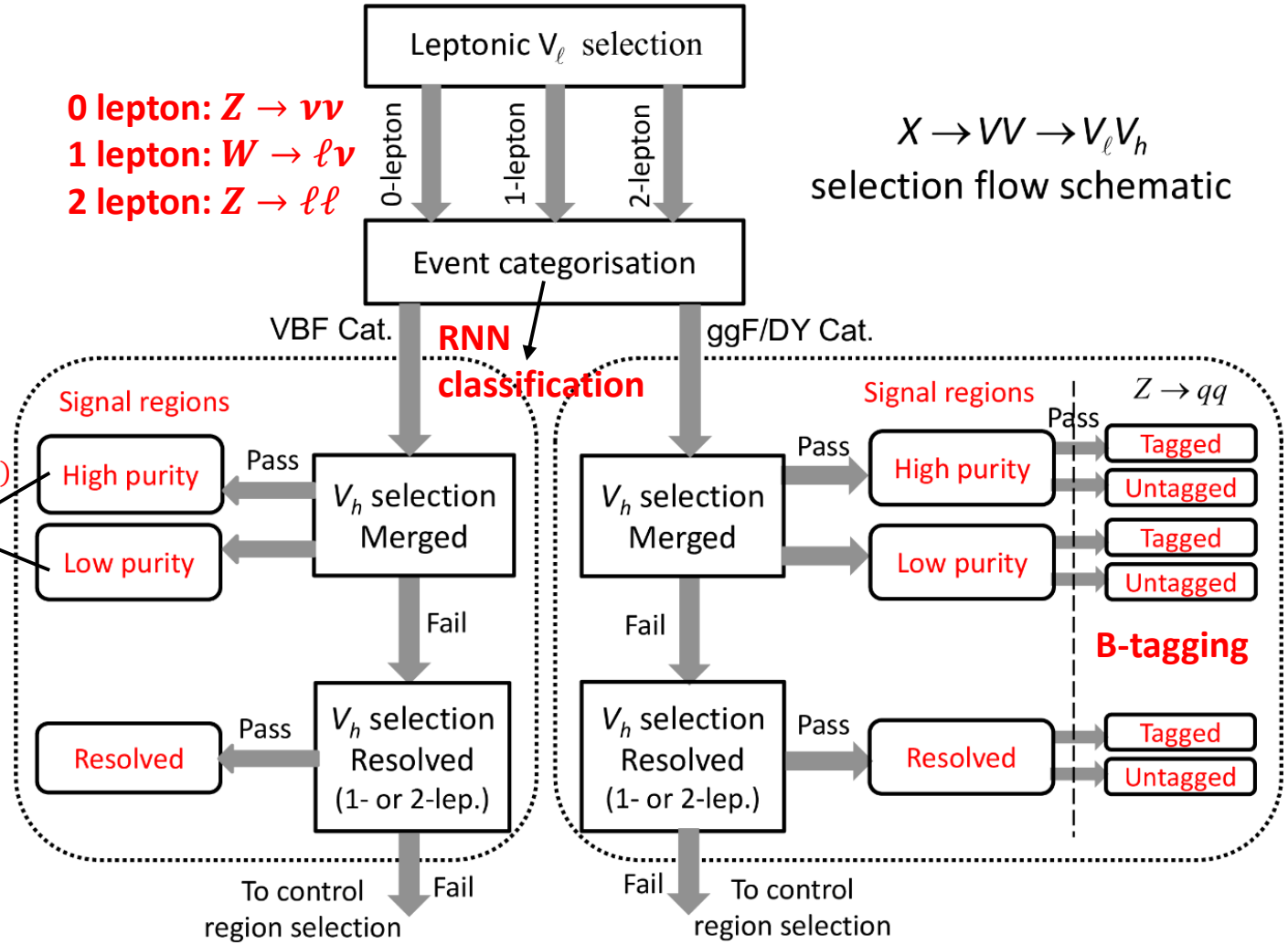

Considered both merged ($V \to J$) and resolved ($V \to jj$) jets

https://arxiv.org/abs/2004.14636, Submitted to EPJC

Search for heavy diboson resonances in semileptonic final states ATLAS

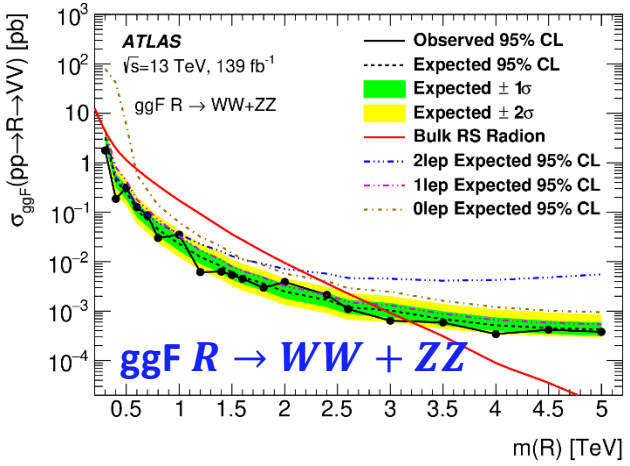

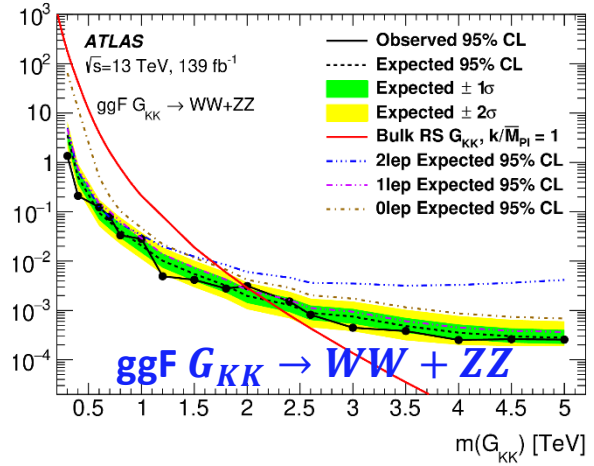

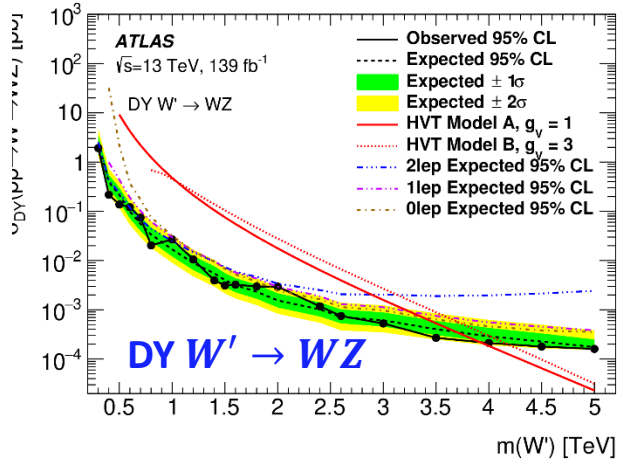

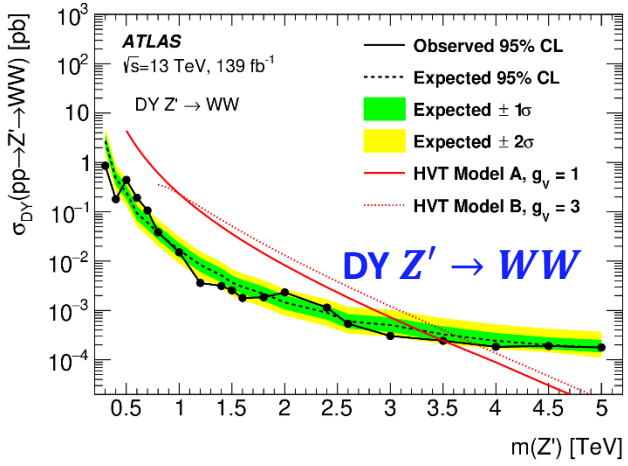

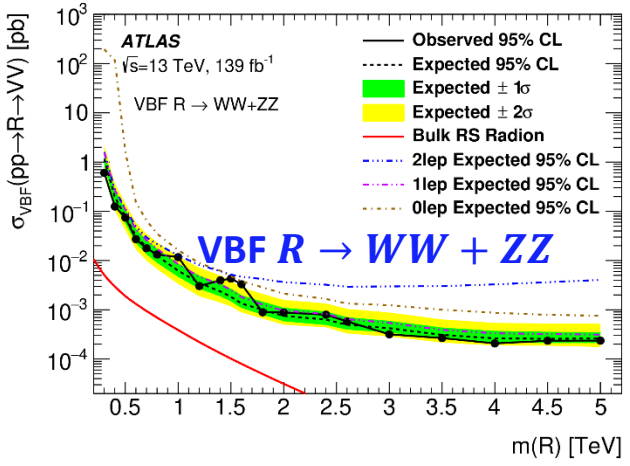

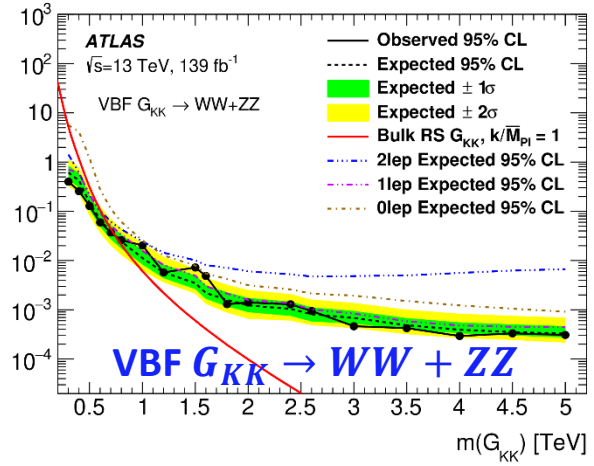

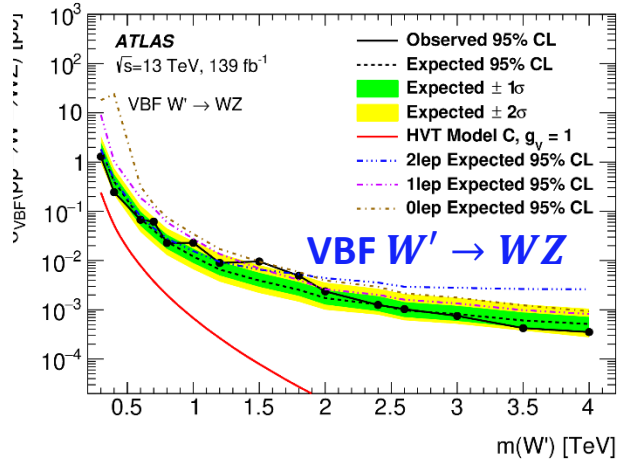

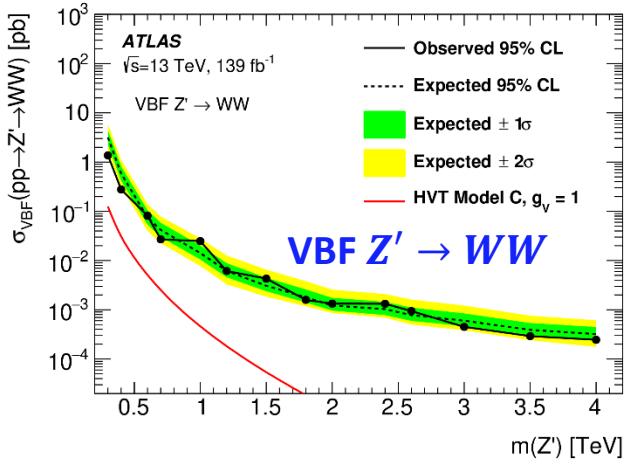

Observed (expected) 95 CL lower limits on the mass, in TeV, of different resonances

Production process	RS radion	HVT			RS graviton
			W'	Z'	
ggF/DY	3.2 (2.9)	Model A	3.9 (3.8)	3.5 (3.4)	2.0 (2.2)
		Model B	4.3 (4.0)	3.9 (3.7)	
VBF	–	Model C	–	–	0.76 (0.77)

Dijet resonance search with weak supervision ATLAS

Search for resonant new physics using a machine-learning anomaly detection procedure that does not rely on a signal model

Weakly supervised learning:

- **Classification Without Labels (CWoLa)**
  - ✓ **sensitive to plenty of signals**
  - ✓ **avoid large trials factor**
  - ✓ **a smart way of doing 3D bump hunt**
- **Calls for two mixed samples that are statistically identical aside from different class proportions**

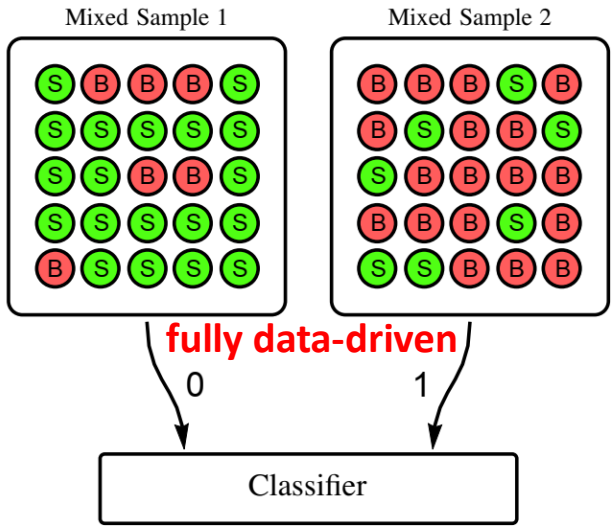

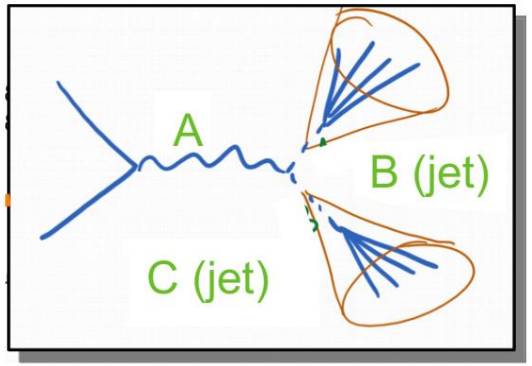

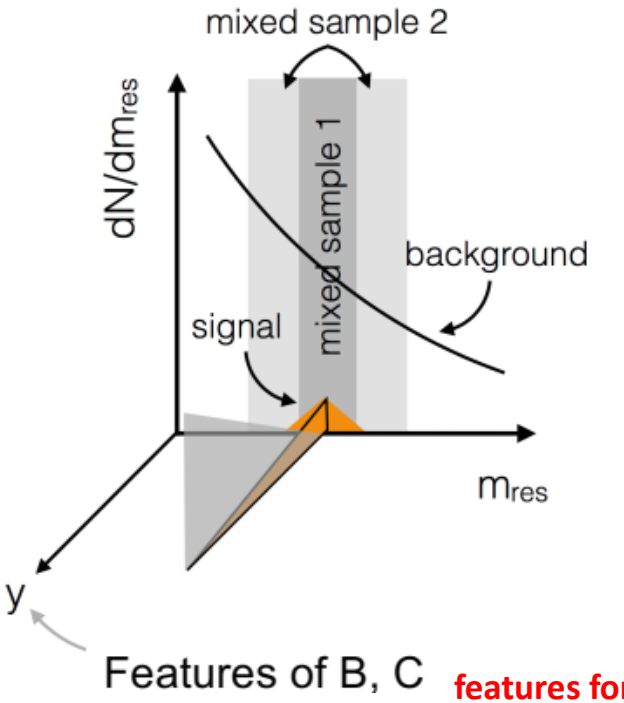

- **Signal regions : m_{JJ} [1.90, 2.28, 2.74, 3.28, 3.94, 4.73, 5.68, 6.81, 8.17] TeV.**
- **In any signal region:**

  signal present: tag that signal and enhance a bump in the m_{JJ} spectrum

  no signal: m_{JJ} spectrum remain smooth after tagging

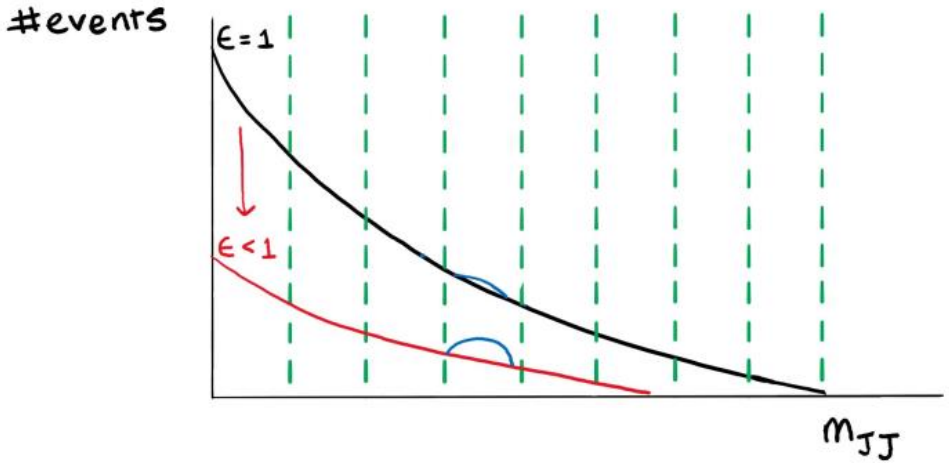

A network is trained to distinguish between a given m_{JJ} signal region and the two neighboring sideband regions

features for ML: masses of the two jets.

https://arxiv.org/abs/2005.02983, Submitted to Phys. Rev. Lett.

Dijet resonance search with weak supervision ATLAS

Selection:

1. **At least two large-R jets with $p_T > 200\ GeV$ and $|\eta| < 2.0$ (reduce t-channel)**
2. **At least one jet with $p_T > 500$**
3. **Two leading jets $|\Delta y_{JJ}| < 1.2$, and both with $30\ GeV < m_J < 500\ GeV$**

Decorrelate 1D $m_J = \{m_1, m_2\}$ distribution by percentile scaling

Combine sidebands (weight = 1/N) to further cancel out differences

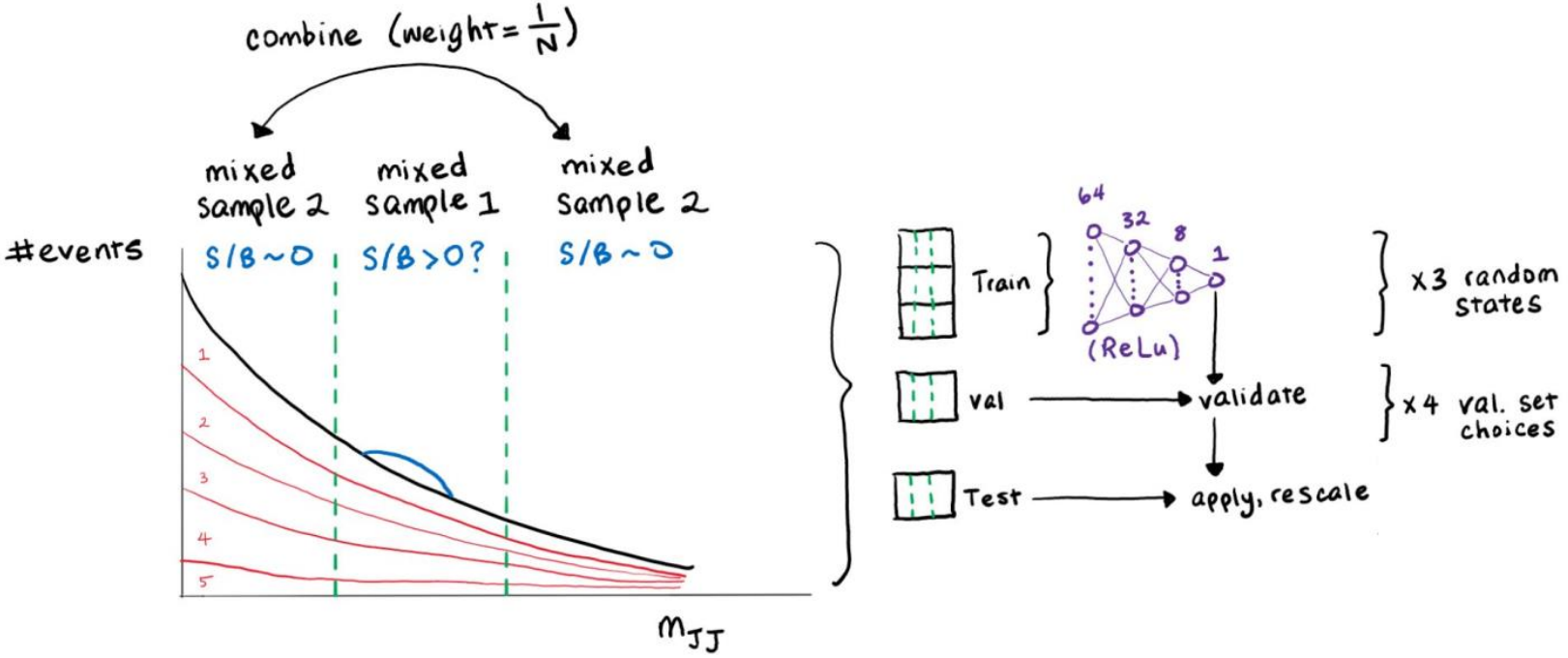

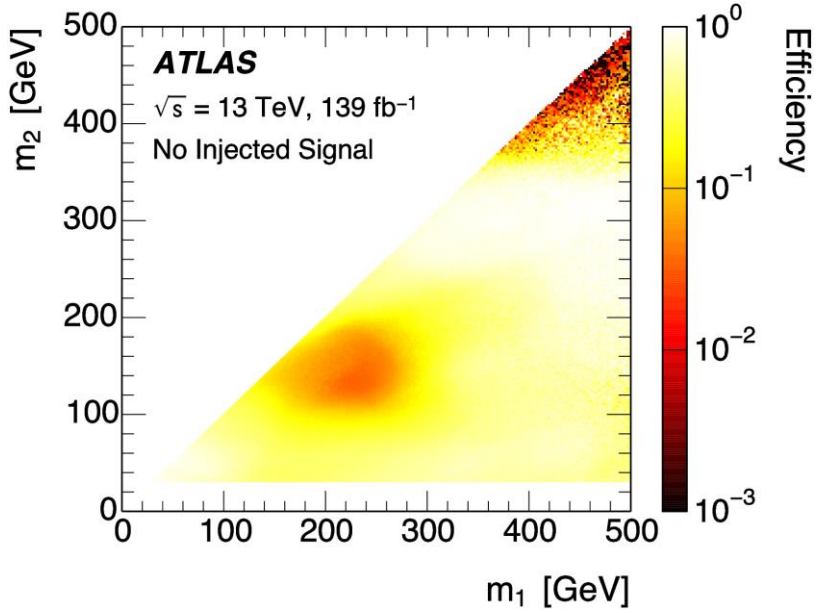

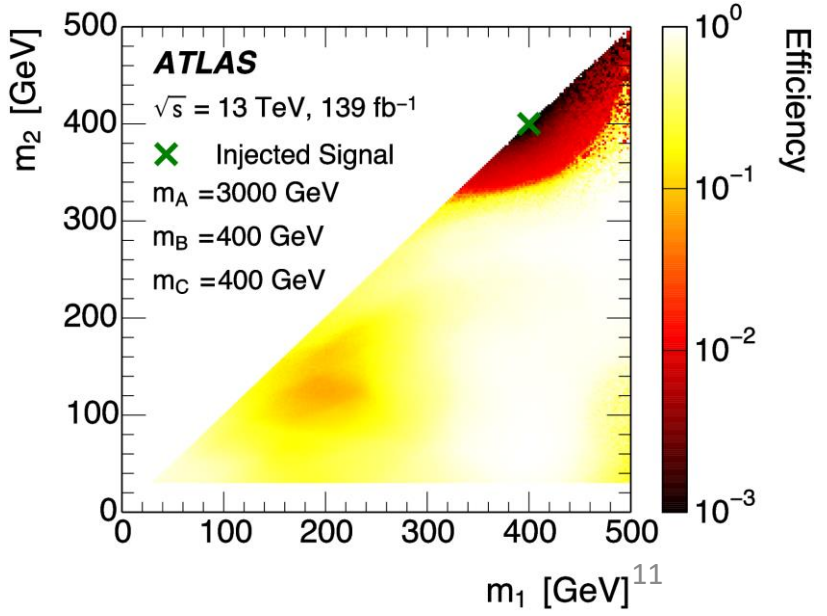

Dijet resonance search with weak supervision ATLAS

Model-dependent fit:

- Train NN with injected signal strength μ:
- Apply NN selection ϵ (depends on μ)
- Let μ be POI and set 95% CL limits in the usual way
- Limit depends on injected signal strength!

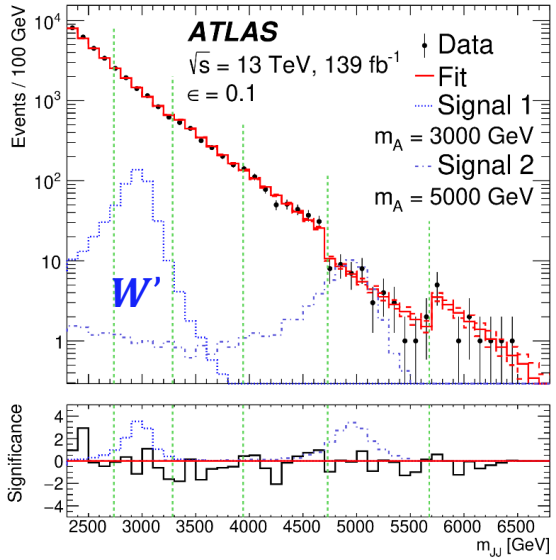

- ✓ First application of fully data-driven machine-learning anomaly detection
- ✓ First search that covers $A \rightarrow BC$ production where all of A, B and C are BSM particles
- ✓ Now only two-dimensional, great potential to extend this method!

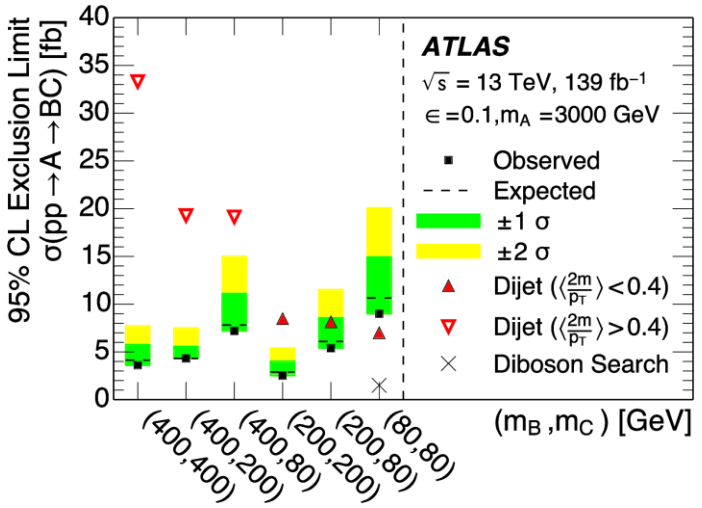

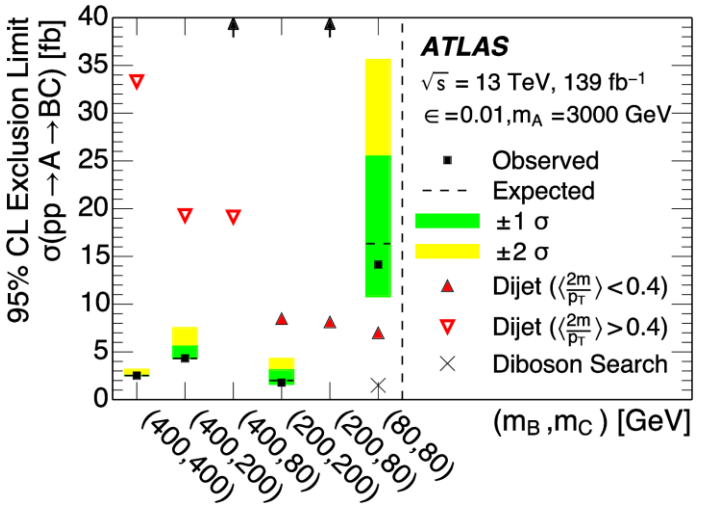

more sensitive than the inclusive di-jet search and extends the coverage of the all-hadronic diboson search to regions away from the SM boson masses.

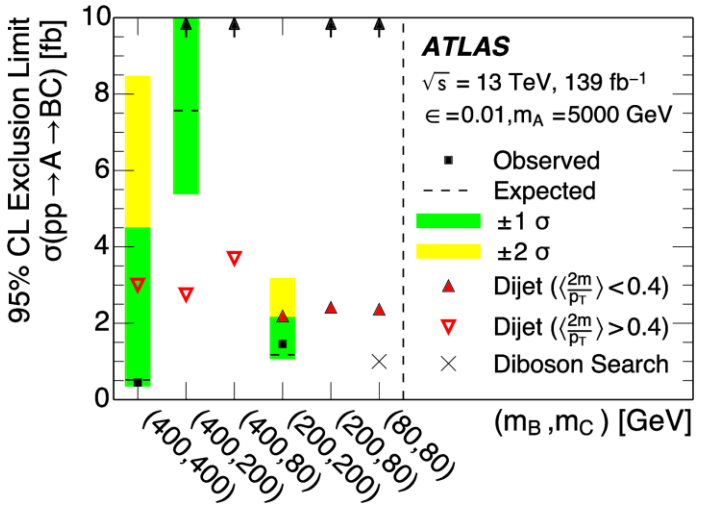

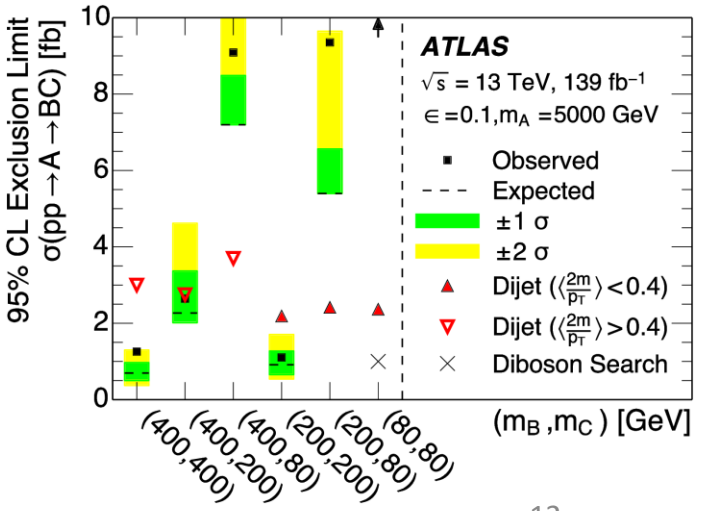

Vector-like quark search

Vector-like Quarks (VLQs) are heavy non-chiral quarks with symmetric left- and right-handed couplings to SM particles

Predicted in many extensions to the SM
(little higgs, composite higgs, warped or extra dimensions, …)

		Decays
Singlet	T	$T \to bW^+, tZ, tH$
	B	$B \to tW^-, bZ, bH$
Doublet	(T,B)	$T \to tZ, tH, B \to bW^-$
	(X,T)	$X \to tW^+, T \to tZ, tH,$
	(B,Y)	$B \to bZ, bH, Y \to bW^-$

Results shown today are focused on Single Production → Sensitive to probe the couplings to SM quarks, e.g. mixing angle θ_L, θ_R

(By comparison, searches for pair-produced VLQs allow limits to be set on VLQ masses which are rather insensitive to the couplings)

	SM quarks	VLQ
electro-weak transformations	same for left- and right-handed	different for left- and right-handed
Obtain mass	Higgs mechanism	new strong sector confinement

Could have a role in stabilizing the Higgs boson mass, and thus offer a potential solution to the hierarchy problem

	Singlets	Doublets	Triplets
	$T_{L,R}$	$(X,T)_{L,R}$	$(X,T,B)_{L,R}$
	$B_{L,R}$	$(T,B)_{L,R}$	$(T,B,Y)_{L,R}$
		$(B,Y)_{L,R}$	

	$\binom{t_L}{b_L}$	t_R	b_R	T	B	$\binom{T}{B}$	$\binom{X}{T}$	$\binom{B}{Y}$
Isospin	$\pm\frac{1}{2}$	0	0	0	0	$+\frac{1}{2}$	$+\frac{1}{2}$	$+\frac{1}{2}$
Hypercharge	$+\frac{1}{3}$	$+\frac{4}{3}$	$-\frac{2}{3}$	$+\frac{2}{3}$	$-\frac{1}{3}$	$+\frac{1}{6}$	$+\frac{7}{6}$	$-\frac{5}{6}$

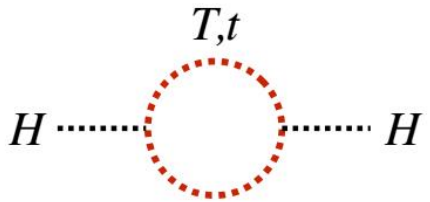

Alternative to SUSY that renders the Higgs natural!

Search for single production of VLQ decaying into Wb ATLAS

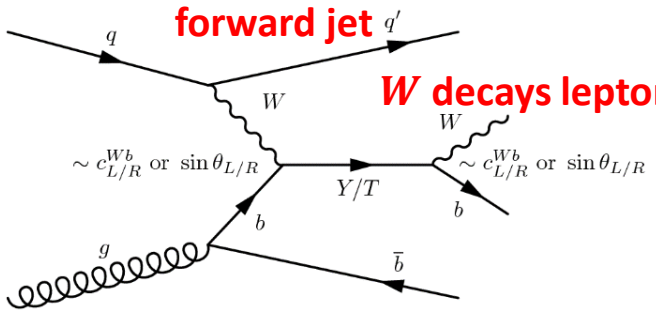

Requirement \ Region	SR	$t\bar{t}$ CR	W+jets CR
Preselection			
Leptons	1		
$E_{\mathrm{T}}^{\mathrm{miss}}$	> 120 GeV		
Central jets ($p_{\mathrm{T}} > 25$ GeV)	≥ 1		
Selection			
b-tagged jets	≥ 1	≥ 1	1
Leading b-jet p_{T}	> 350 GeV	> 200 GeV	> 250 GeV
$\lvert\Delta\phi$(lepton,b-tagged jet)$\rvert$	> 2.5	> 2.5	< 2.5
Jets ($p_{\mathrm{T}} > 75$ GeV) with ΔR (jet, b-tagged jet) < 1.2 or ΔR (jet, b-tagged jet) > 2.7	0	≥ 1	–
ΔR (lepton, jets)	> 2.0	–	> 2.0
Forward jets ($p_{\mathrm{T}} > 40$ GeV)	≥ 1	≥ 1	–

Sizeable interference effects between the amplitude for VLQ signal production and the SM are considered:

1. ***T*-quark production in a *T* singlet model, with only a left-handed coupling, interfere with t-channel single top**
2. ***Y*-quark production in a (*T*, *B*, *Y*) triplet or (*B*, *Y*) doublet model with only a left-handed coupling or right-handed coupling, interfere with electroweak $W^- bq$**

$$\sigma_{\mathrm{tot}}^{\mathrm{NLO}} = K_{\mathrm{SM}}\sigma_{\mathrm{SM}}^{\mathrm{LO}} + K_{\mathrm{VLQ}}\sigma_{\mathrm{VLQ}}^{\mathrm{LO}} + \sqrt{K_{\mathrm{SM}} \cdot K_{\mathrm{VLQ}}}\sigma_{\mathrm{I}}^{\mathrm{LO}}.$$

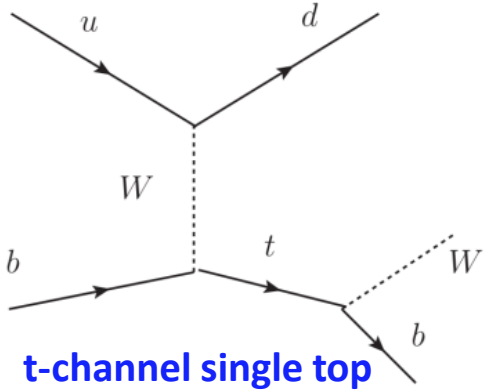

t-channel single top

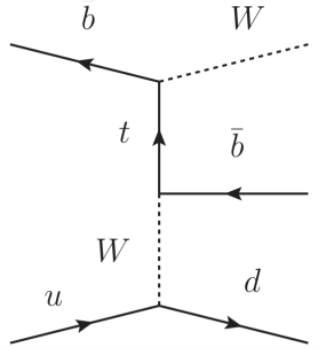

electroweak $W^- bq$

https://arxiv.org/abs/1812.07343, JHEP 05 (2019) 164

Search for single production of VLQ decaying into Wb ATLAS

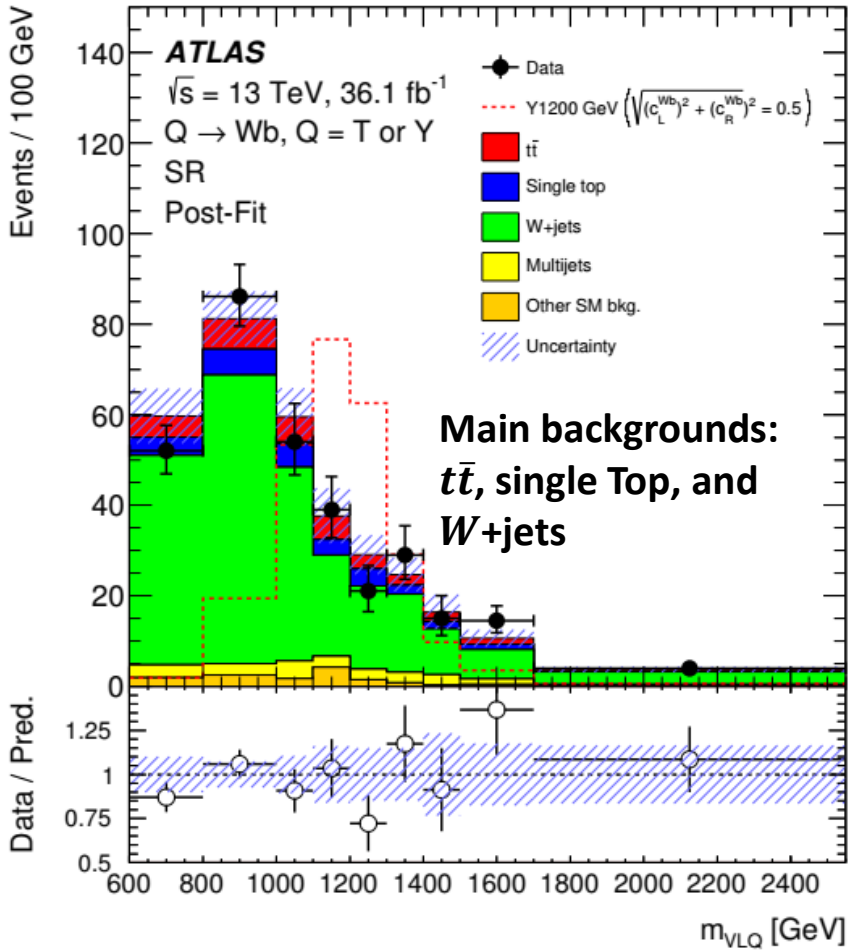

Main backgrounds: $t\bar{t}$, single Top, and W+jets

competitive with the indirect constraints for VLQ masses between 800 GeV and 1250 GeV

Coupling limits are extracted with reweighting factors of interference

$$r(m_{Wb}; c, c_0) = \frac{K_{\mathrm{VLQ}} f_{\mathrm{VLQ}}(m_{Wb}; c) + \sqrt{K_{\mathrm{SM}} \cdot K_{\mathrm{VLQ}}} f_{\mathrm{I}}(m_{Wb}; c)}{f_{\mathrm{VLQ}}(m_{Wb}; c_0)},$$

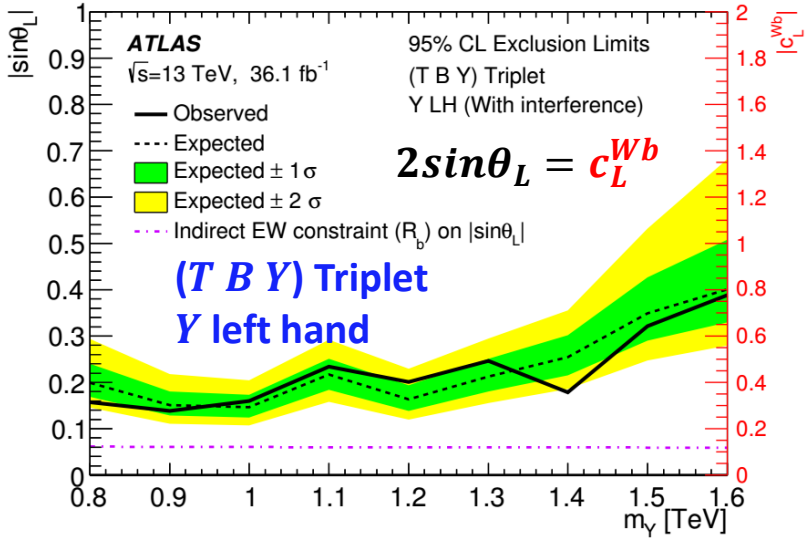

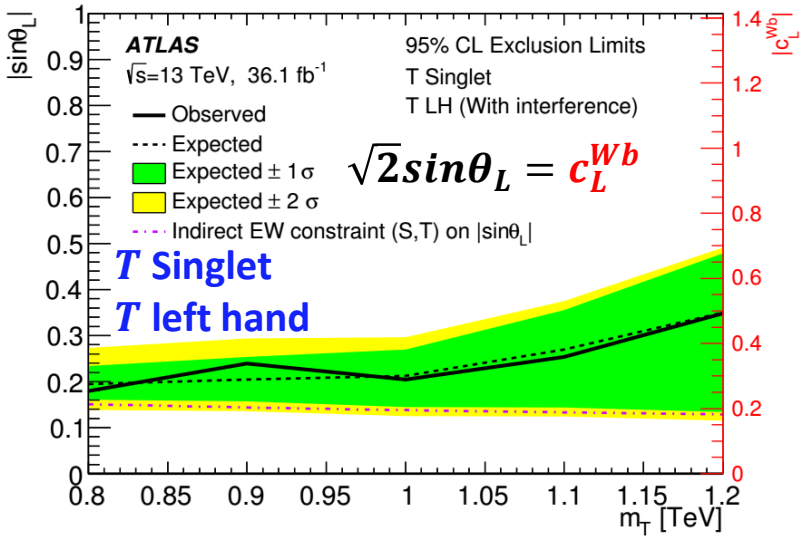

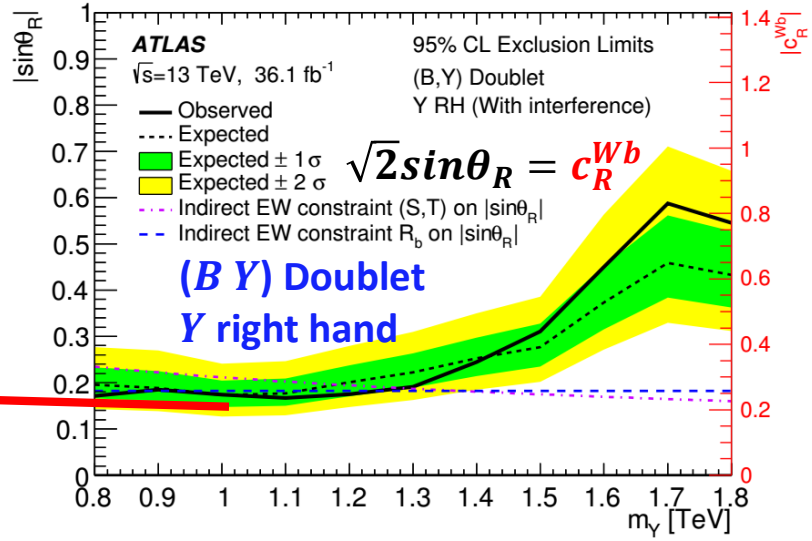

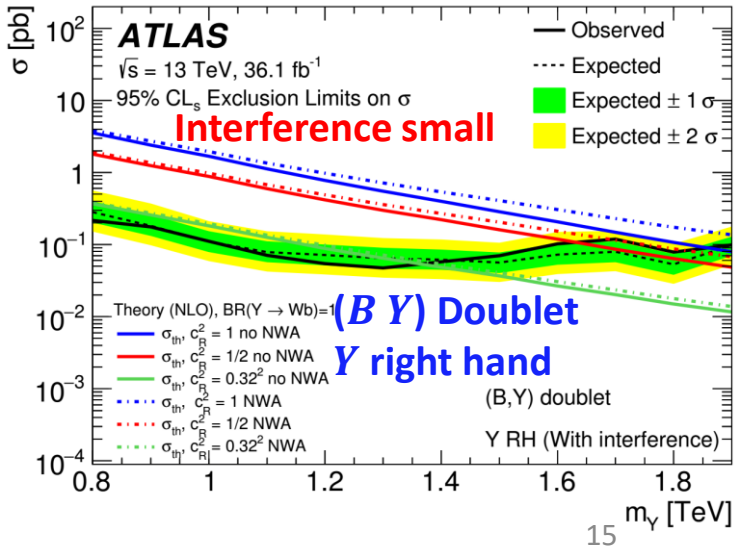

Search for large MET with one top-quark ATLAS

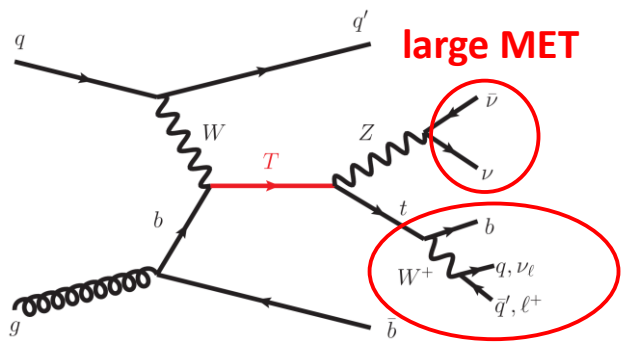

large MET

collimated into a large-R jet

Final discriminate: transverse mass of (E_T^{miss}, J)

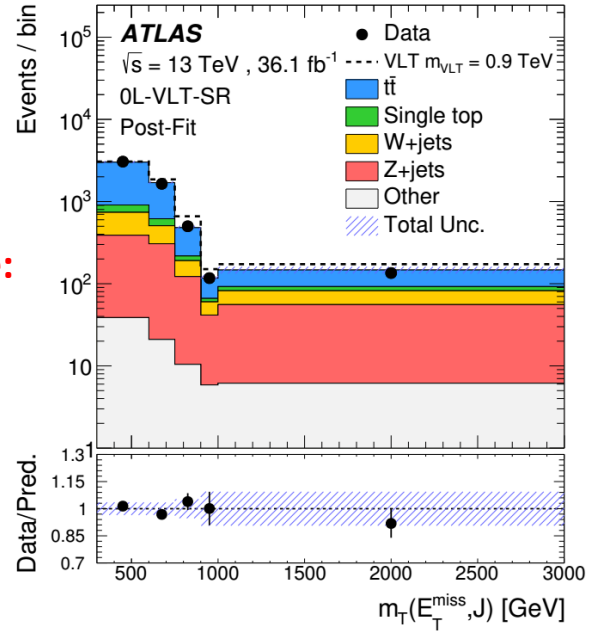

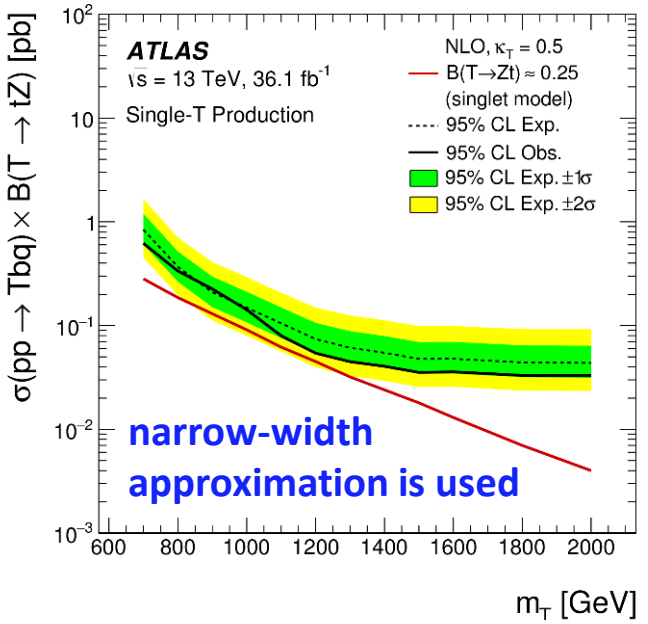

Main backgrounds: $t\bar{t}$, single Top, W+jets, and Z+jets

Selections (hadronic channel)	0L-DM-SR	0L-VLT-SR
Number of forward jets	= 0	≥ 1
Number of leptons	= 0	
$E_{\mathrm{T}}^{\mathrm{miss}}$ [GeV]	> 200	
Number of large-R jets	≥ 1	
Number of top-tagged jets	≥ 1	
$\Delta\Phi(E_{\mathrm{T}}^{\mathrm{miss}}, J)$	> $\frac{\pi}{2}$	
Number of track-jets	≥ 1	
Number of b-tagged track-jets	= 1	
Veto jet (masked tile-calo)	-	
$\Omega = \frac{E_{\mathrm{T}}^{\mathrm{miss}} - p_{\mathrm{T}}(J)}{E_{\mathrm{T}}^{\mathrm{miss}} + p_{\mathrm{T}}(J)}$	> −0.3	
$\Delta\Phi_{\mathrm{min}}(E_{\mathrm{T}}^{\mathrm{miss}}$, calo jets)	> 1.0	

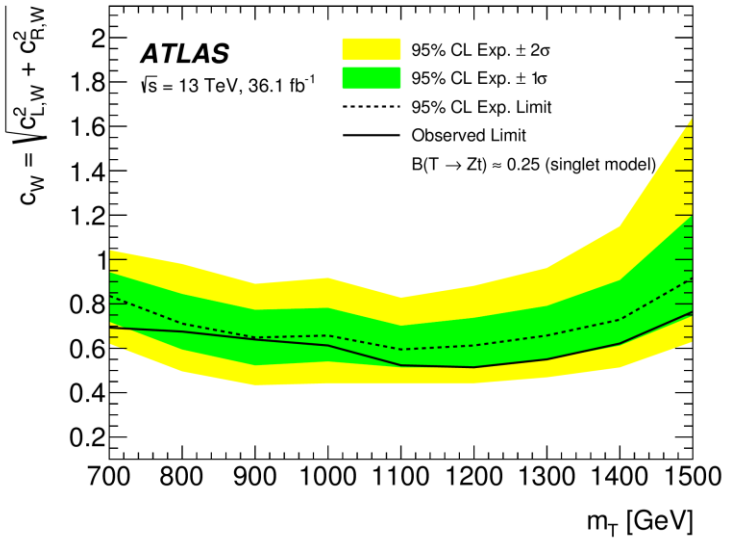

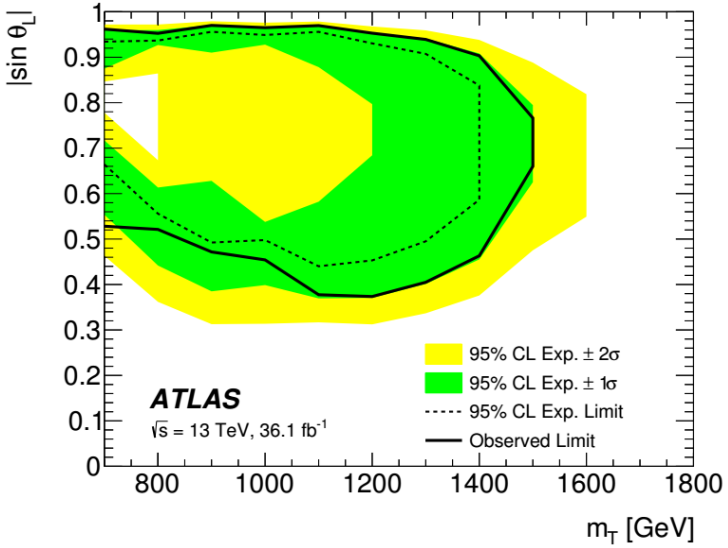

https://arxiv.org/abs/1812.09743, JHEP 05 (2019) 41

Electroweak production of vector-like T quark fully hadronic final states CMS

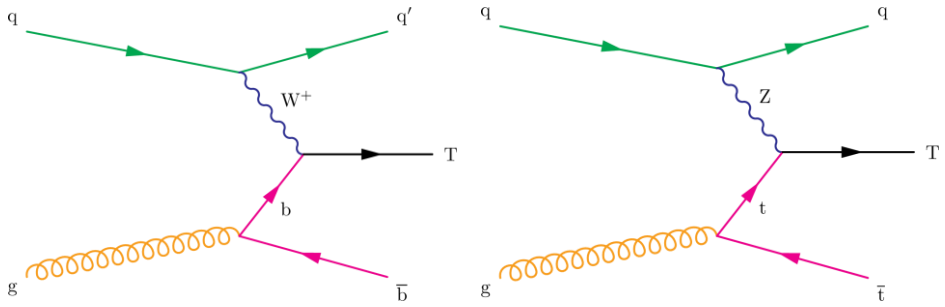

Signature:

1. $T \to tH$ and $T \to tZ$ with $X \to bb$ ($X = H, Z$) and top decays all hadronically
2. Looking for a M_{tX} peak
3. Two mass range considered:
   - **Low-mass search** (T mass 0.6 to 1.2 TeV): Invariant mass of 5-jets (≥3 b tagged)
   - **High-mass search** (T mass > 1 TeV): Invariant mass of 2 large-R jets

Main backgrounds: multijet and $t\bar{t}$

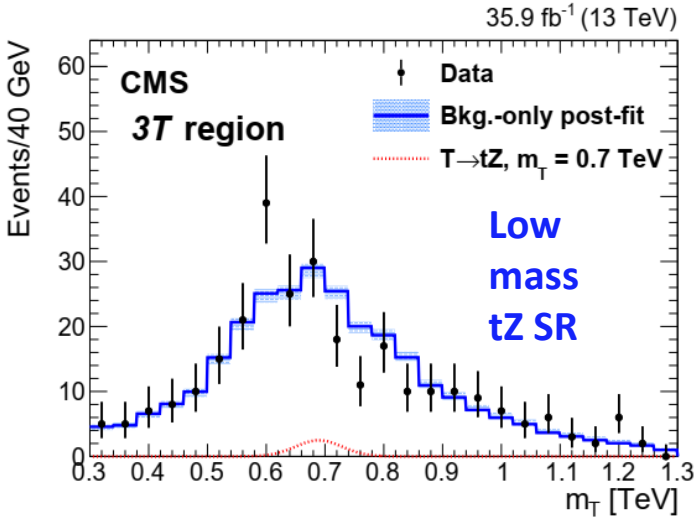

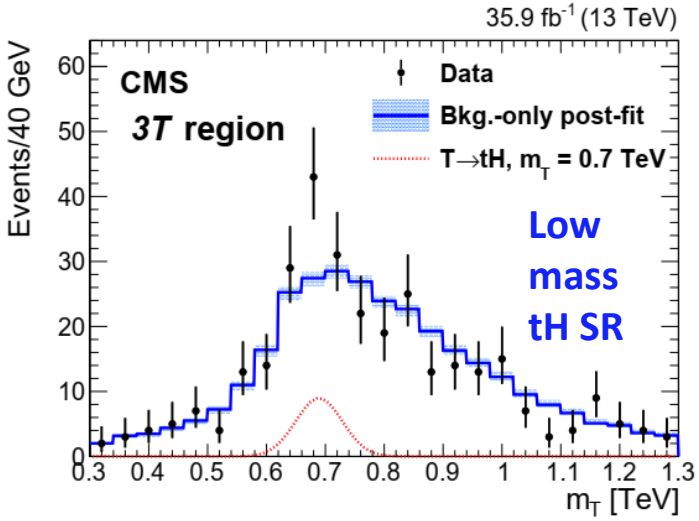

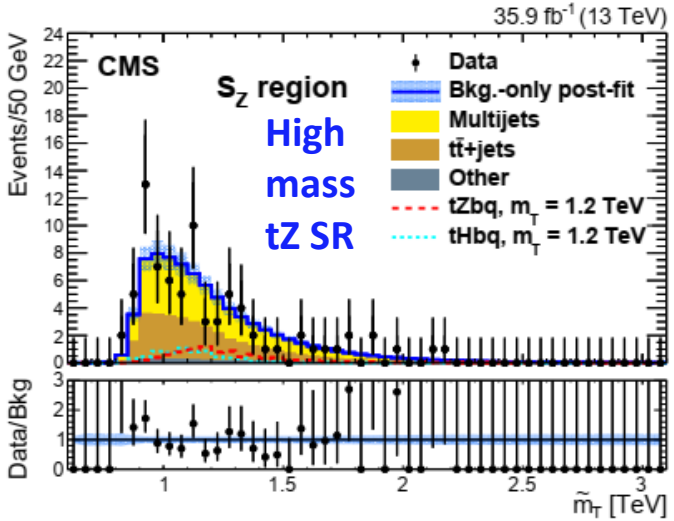

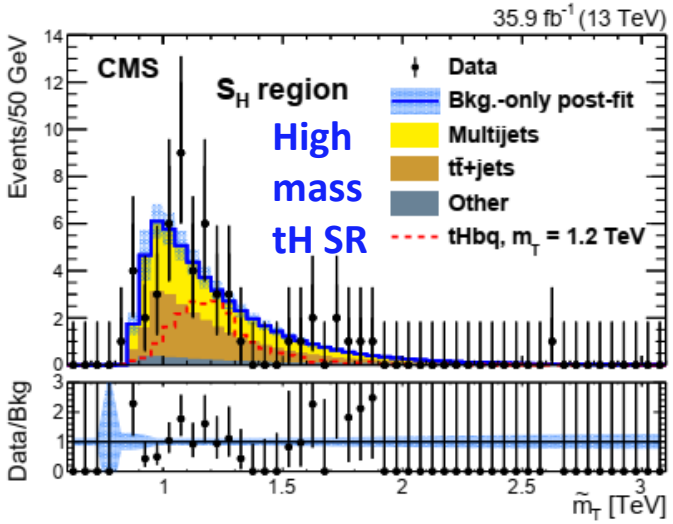

https://arxiv.org/abs/1909.04721, JHEP 01 (2020) 036

Electroweak production of vector-like T quark fully hadronic final states CMS

T masses below 1 TeV, the models with a bottom quark are strongly constrained

expected sensitivity up to 1.28 TeV

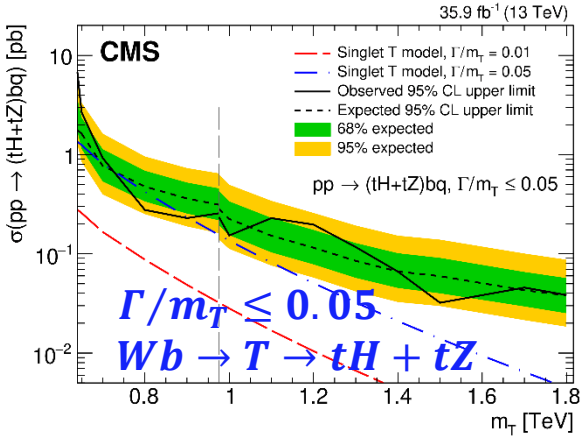

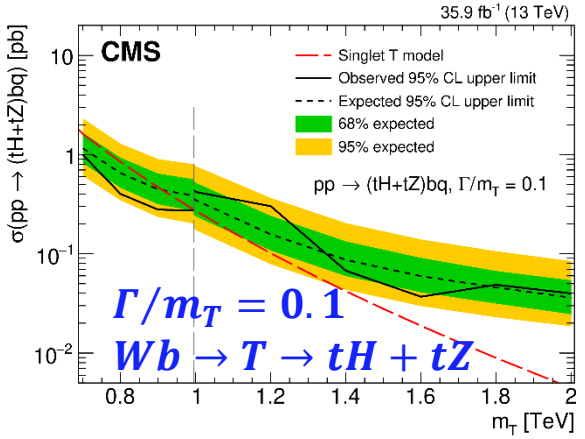

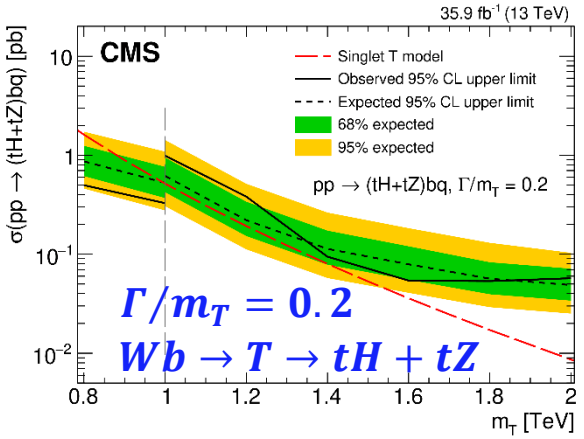

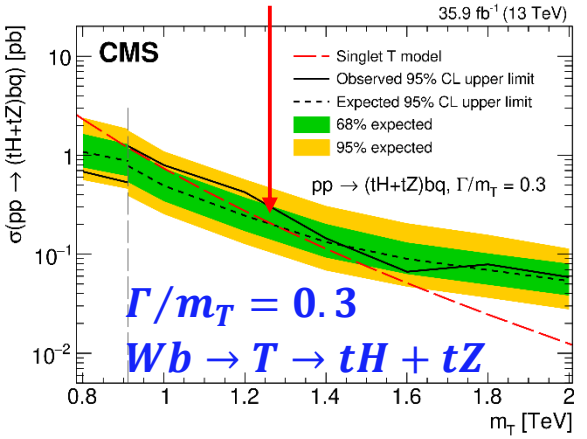

expected sensitivity up to 0.82 TeV

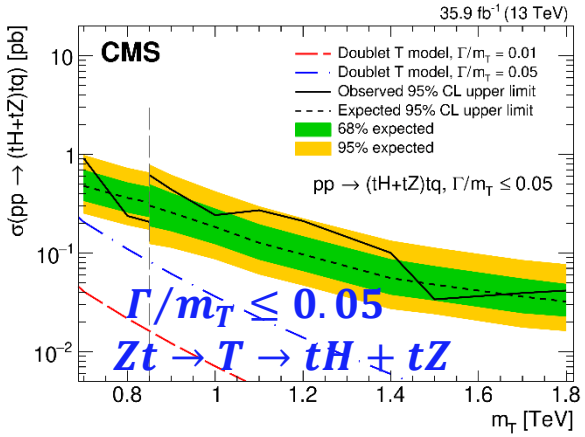

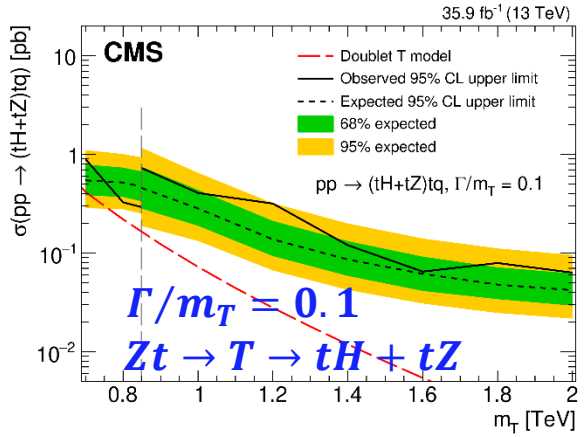

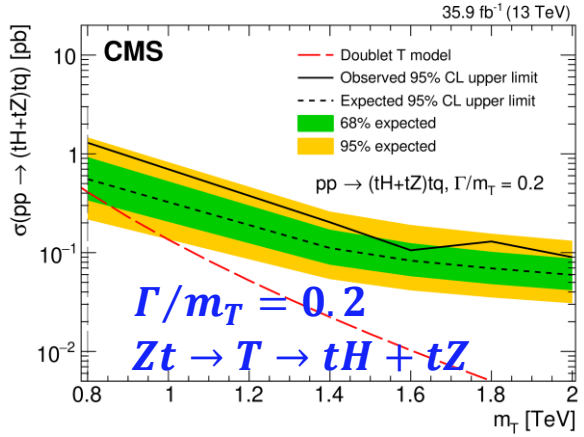

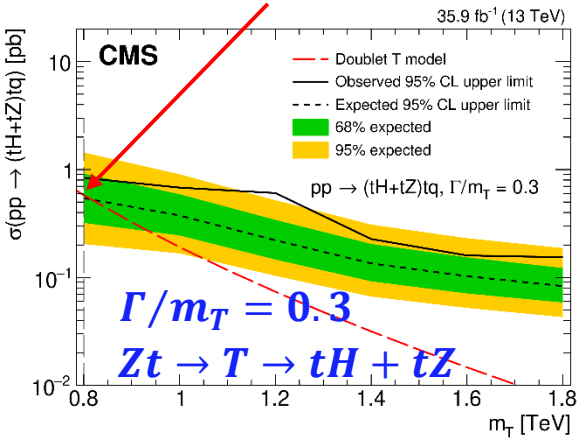

Showing limits of whichever of the two searches (high mass or low mass) for each mass with best estimated expected sensitivity

- ✓ **Significantly more sensitive for $T \to tH$ compared with previous searches**
- ✓ **Gives the first constraints using this production mode on $T \to tZ$ for hadronic decays of the Z boson**

Summary

No evidence for New Physics yet

Limits are set for multiple theory models of diboson resonance and VLQ, pushes resonance masses higher

Combination efforts have been made to give a bigger picture for diboson searches

New techniques are developed to better distinguish $W/Z/H$ from SM BKG

much more to come with more analysis scrutinizing full Run II data!

Thanks!

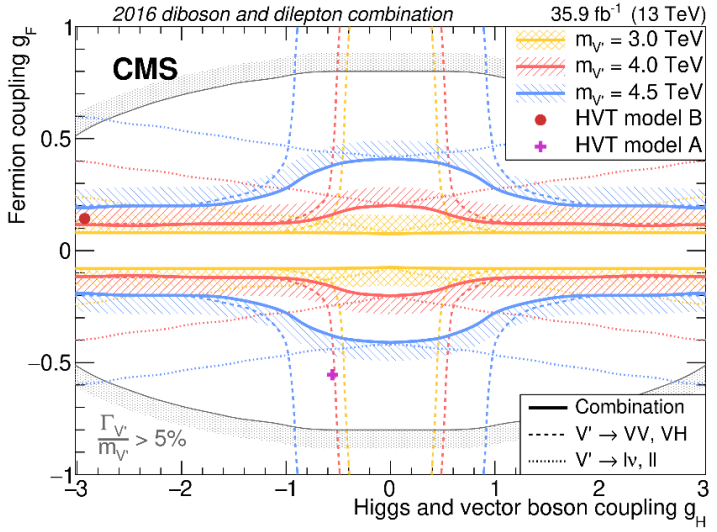

https://arxiv.org/abs/1906.00057

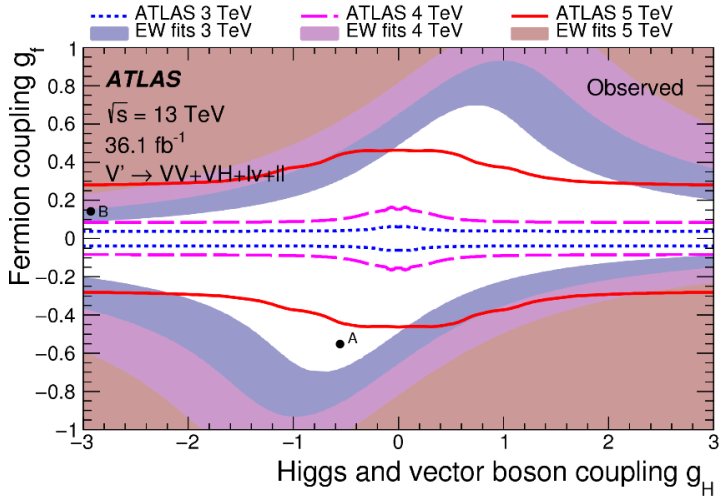

https://arxiv.org/abs/1808.02380

back up

Search for VH resonances in hadronic final states ATLAS

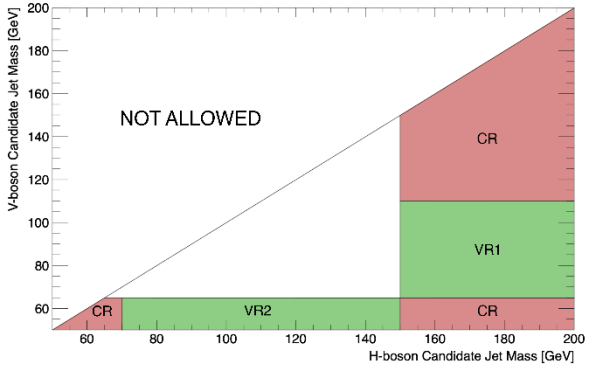

Figure 3: Illustration of control and validation regions, defined by the masses of the H-boson and V-boson candidates. The regions VR1 and VR2 are further split into two regions each, according to the n_{trk} requirement on the V-boson candidate. The same definitions are applied across the number of b-tags (0-, 1-, and 2-tag categories).

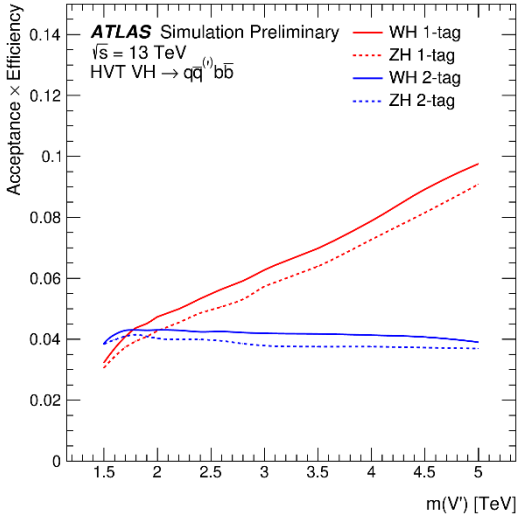

Figure 2: Signal acceptance times efficiency as a function of the resonance mass, for events in the WH (solid lines) and ZH (dashed lines) signal regions, in the 1-tag and 2-tag categories, with respect to the total number of generated events in each sample. The HVT MC samples include only $V' \to VH$ decays with $V \to q\bar{q}^{(\prime)}$ and $H \to b\bar{b}$ or $c\bar{c}$.

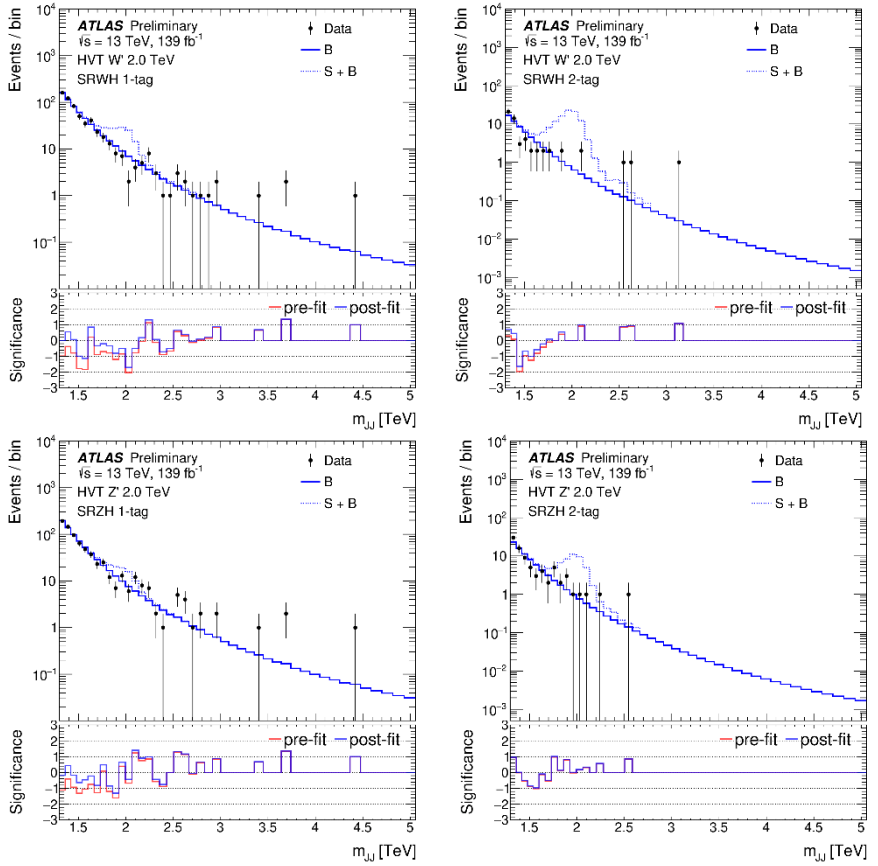

Figure 5: Dijet mass distributions in the WH (top) and ZH (bottom) signal regions, after the likelihood fit on events from 1-tag (left) and 2-tag (right) categories. The black points correspond to data and the solid blue histogram to the post-fit background prediction. The WH and ZH signal regions are not orthogonal. The expected signal distributions for a V' boson with mass of 2 TeV are also shown (dashed histograms). The width of each bin is variable and corresponds to the experimental mass resolution. Distributions of the significance of the observed deviations from the expected background are presented in the bottom panels before and after the fit. The significance calculation assumes Poisson probabilities and only accounts for statistical fluctuations.

multi-dimensional search for diboson resonances in the dijet final state CMS

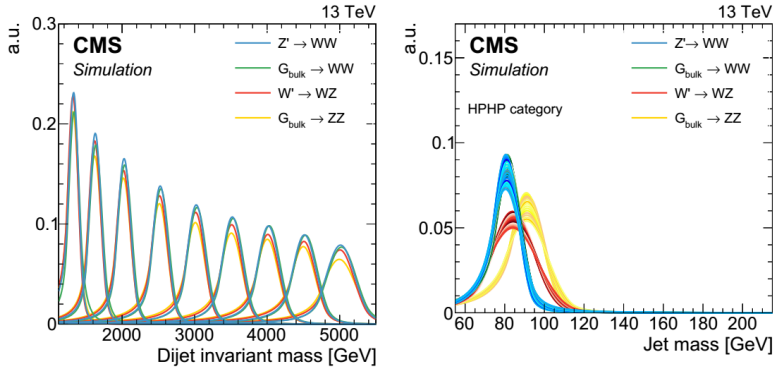

Figure 7: The final m_{jj} (left) and m_{jet1} (right) signal shapes extracted from the parameterization of the dCB function. The same m_{jj} shapes are used for both purity categories. The jet mass distributions are shown for a range of resonance masses between 1.2 and 5.2 TeV for one of the two jets in the events in the HPHP category. Because the jets are labelled randomly, the jet mass distributions for the second jet are essentially the same as the one shown. The distributions for a G_{bulk} decaying to WW have the same shapes as those for the Z′ signal and are therefore not visible.

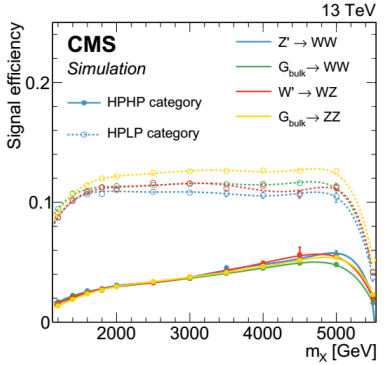

Figure 6: Total signal efficiency as a function of m_X after all selections are applied, for signal models with a Z′ decaying to WW, G_{bulk} decaying to WW, W′ decaying to WZ , and G_{bulk} decaying to ZZ. The denominator is the number of generated events. The solid and dashed lines show the signal efficiencies for the HPHP and HPLP categories, respectively. The decrease in efficiency between 5.0 and 5.5 TeV is due to the requirement $m_{jj} < 5500$ GeV.

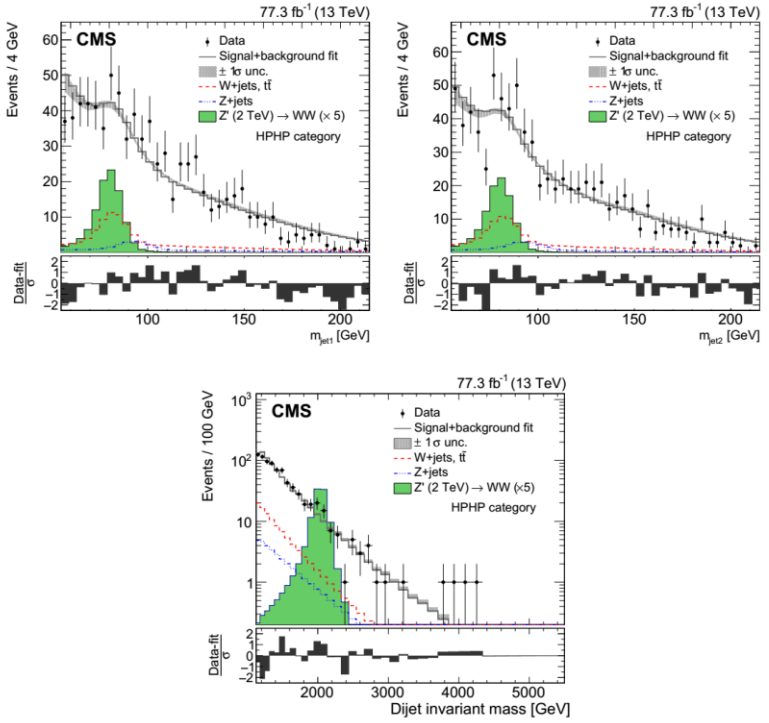

Figure 10: For the HPHP category: comparison between the signal+background fit and the data distributions of m_{jet1} (upper left), m_{jet2} (upper right), and m_{jj} (lower). The background shape uncertainty is shown as a gray shaded band, and the statistical uncertainties of the data are shown as vertical bars. An example of a signal distribution is overlaid, where the number of expected events is scaled by a factor of 5. Shown below each mass plot is the corresponding pull distribution (Data-fit)/σ, where $\sigma = \sqrt{\sigma^2_{data} - \sigma^2_{fit}}$ for each bin to ensure a Gaussian pull-distribution, as defined in Ref. [83].

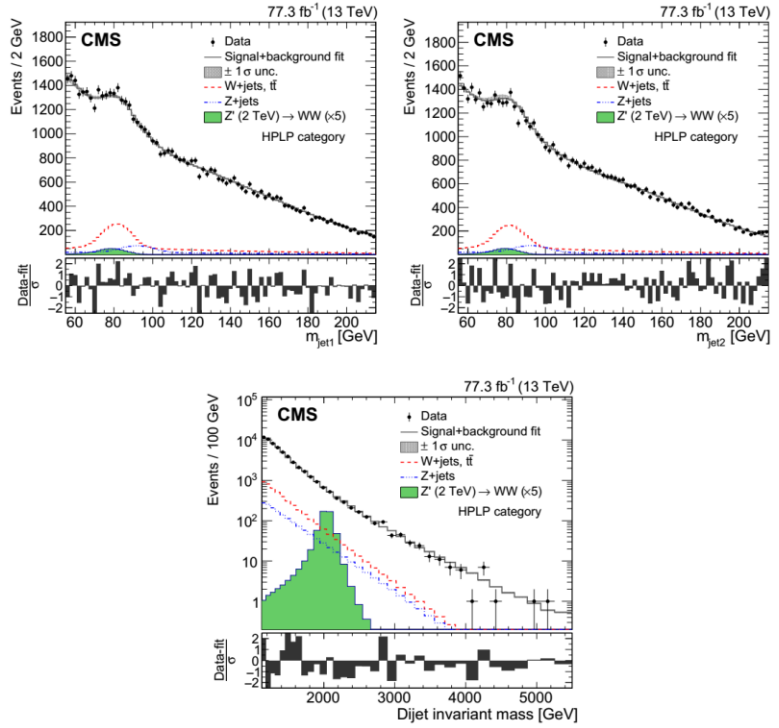

Figure 11: For the HPLP category: comparison between the signal+background fit and the data distributions of m_{jet1} (upper left), m_{jet2} (upper right), and m_{jj} (lower). The background shape uncertainty is shown as a gray shaded band, and the statistical uncertainties of the data are shown as vertical bars. An example of a signal distribution is overlaid, where the number of expected events is scaled by a factor of 5. Shown below each mass plot is the corresponding pull distribution (Data-fit)/σ, where $\sigma = \sqrt{\sigma^2_{data} - \sigma^2_{fit}}$ for each bin to ensure a Gaussian pull-distribution, as defined in Ref. [83].

Heavy resonance HH bbbb ATLAS

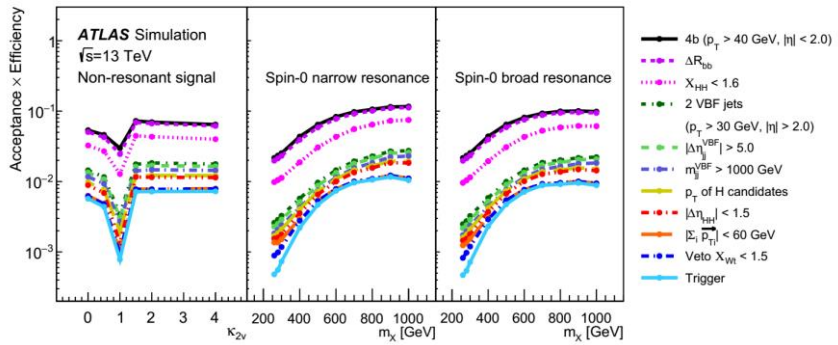

Figure 2: Cumulative acceptance times efficiency at each stage of the event selection, as detailed in Section 5. The number of events surviving the selection divided by the number of generated events is reported separately for the non-resonant signal as a function of the κ_{2V} coupling modifier and for the narrow- and broad-width resonance production hypotheses as a function of the generated mass.

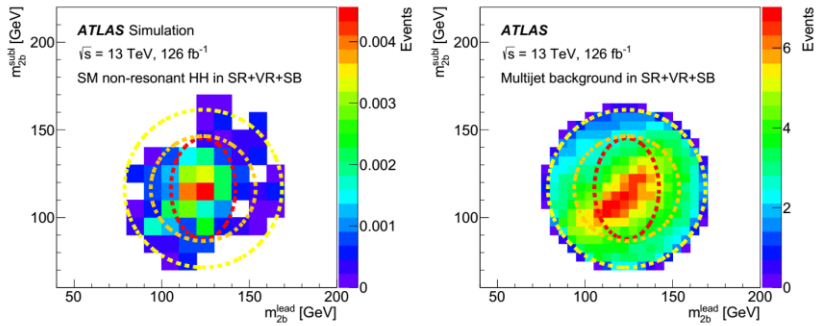

Figure 3: Two-dimensional mass regions used in the analysis. The signal region is inside the inner (red) dashed curve, the validation region is outside the signal region and within the intermediate (orange) circle, and the sideband is outside the validation region and within the outer (yellow) circle. The regions are shown for (a) simulated events from the SM non-resonant HH process and (b) the estimated multijet background.

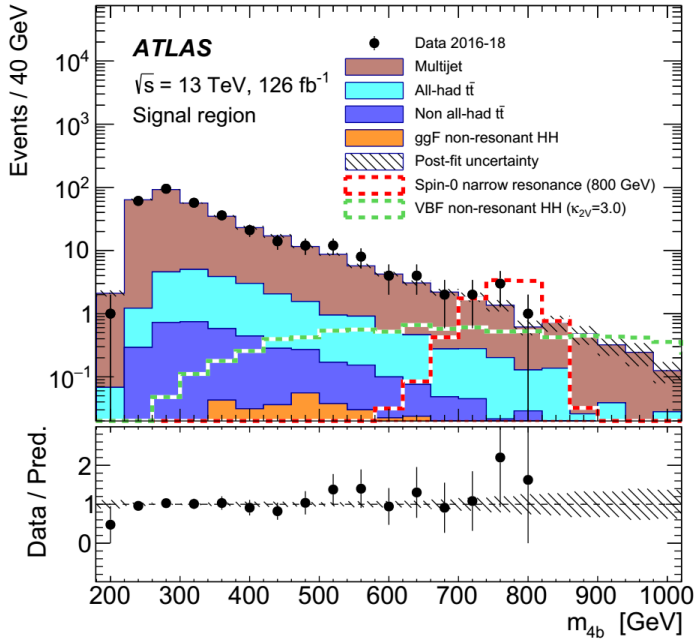

Figure 4: Post-fit mass distribution of the HH candidates in the signal region. The expected background is shown after the profile-likelihood fit to data with the background-only hypothesis; the narrow-width resonant signal at 800 GeV and the non-resonant signal at $\kappa_{2V} = 3$ are overlaid, both normalised to the corresponding observed upper limits on the cross-section. The lower panel shows the ratio of the observed data to the estimated SM background. The distribution of events is shown per mass interval corresponding to the bin width of 40 GeV, while the overflow events are included in the last bin.

Heavy resonance HH bbqqlv CMS

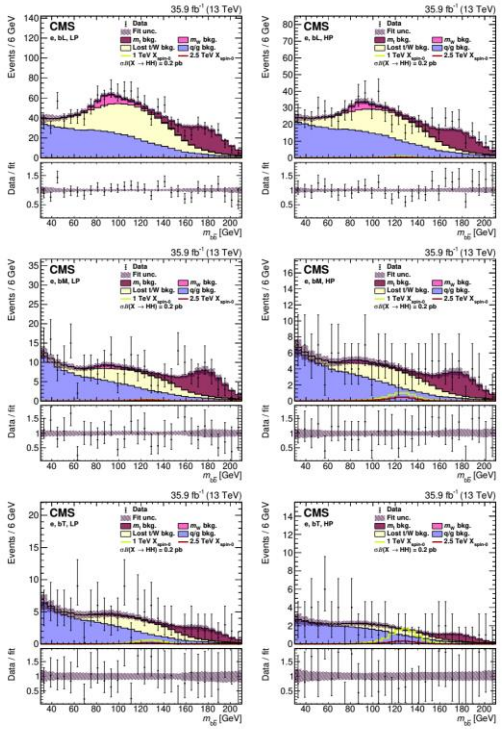

Figure 3. The fit result compared to data projected in $m_{b\bar{b}}$ for the electron event categories. The fit result is the filled histogram, with the different colors indicating different background categories. The background shape uncertainty is shown as the hatched band. Example spin-0 signal distributions for m_X of 1 and 2.5 TeV are shown as solid lines, with the product of the cross section and branching fraction to two Higgs bosons set to 0.2 pb. The lower panels show the ratio of the data to the fit result.

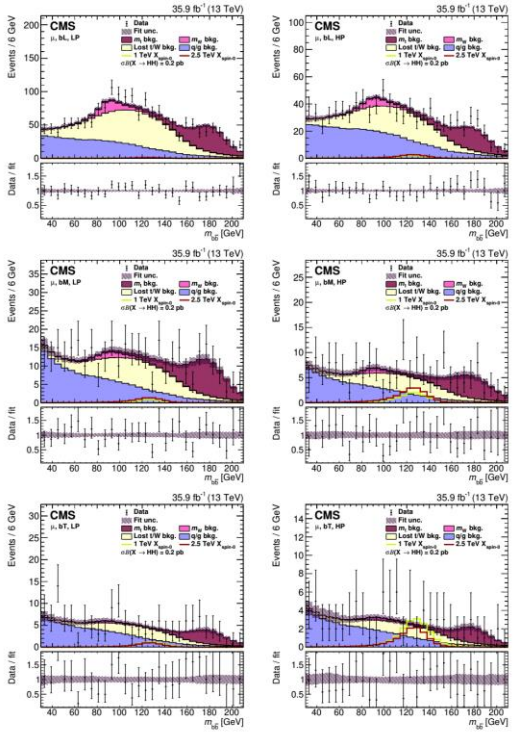

Figure 4. The fit result compared to data projected in $m_{b\bar{b}}$ for the muon event categories. The fit result is the filled histogram, with the different colors indicating different background categories. The background shape uncertainty is shown as the hatched band. Example spin-0 signal distributions for m_X of 1 and 2.5 TeV are shown as solid lines, with the product of the cross section and branching fraction to two Higgs bosons set to 0.2 pb. The lower panels show the ratio of the data to the fit result.

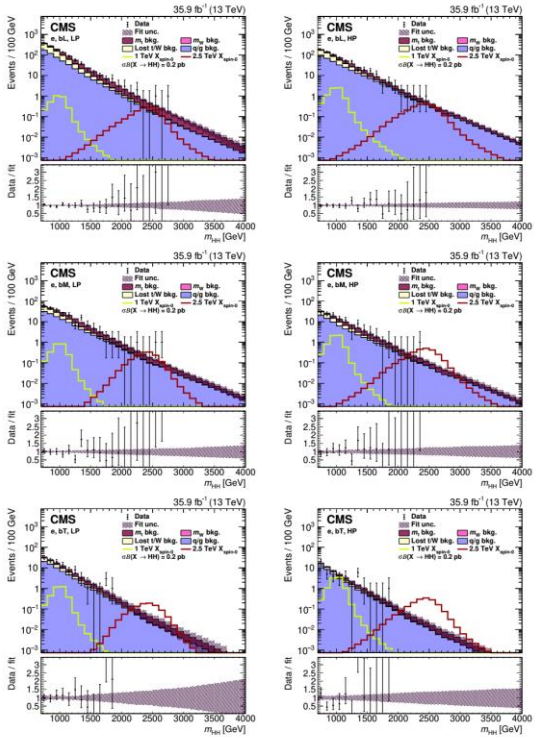

Figure 5. The fit result compared to data projected in m_{HH} for the electron event categories. The fit result is the filled histogram, with the different colors indicating different background categories. The background shape uncertainty is shown as the hatched band. Example spin-0 signal distributions for m_X of 1 and 2.5 TeV are shown as solid lines, with the product of the cross section and branching fraction to two Higgs bosons set to 0.2 pb. The lower panels show the ratio of the data to the fit result.

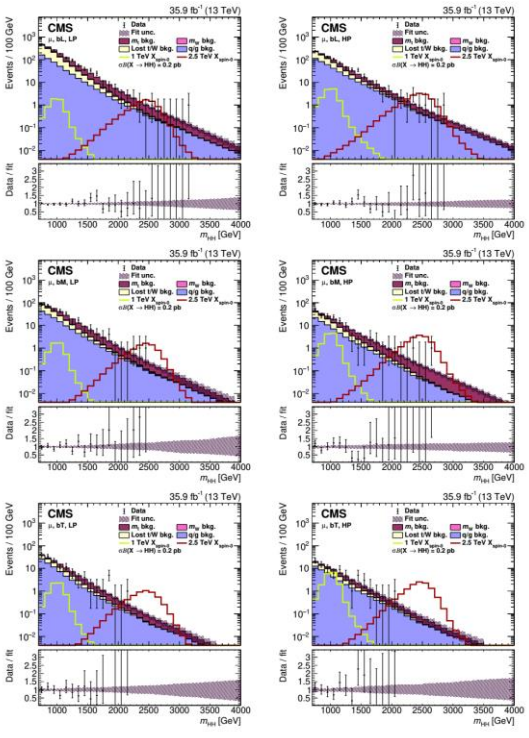

Figure 6. The fit result compared to data projected in m_{HH} for the muon event categories. The fit result is the filled histogram, with the different colors indicating different background categories. The background shape uncertainty is shown as the hatched band. Example spin-0 signal distributions for m_X of 1 and 2.5 TeV are shown as solid lines, with the product of the cross section and branching fraction to two Higgs bosons set to 0.2 pb. The lower panels show the ratio of the data to the fit result.

Search for heavy diboson resonances in semileptonic final states ATLAS

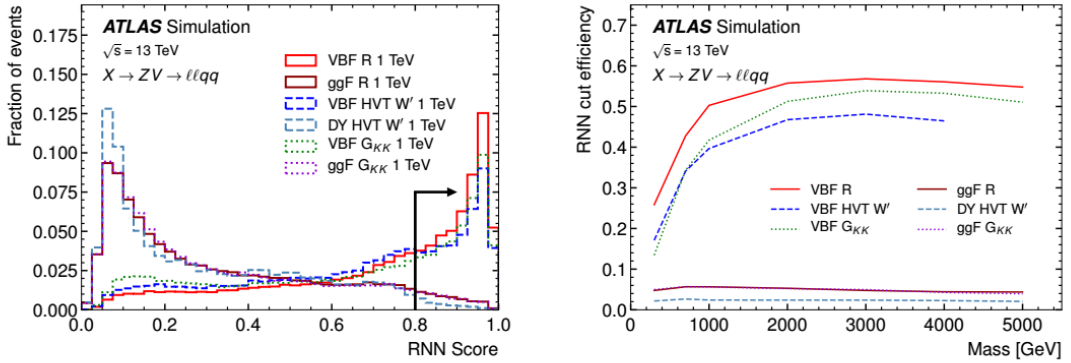

(a) (b)

Figure 3: (a) RNN score distributions for the production of a 1 TeV resonance in the signal models considered for this search; (b) The fractions of signal events passing the VBF requirement on the RNN score as functions of the resonance mass for both VBF and ggF production.

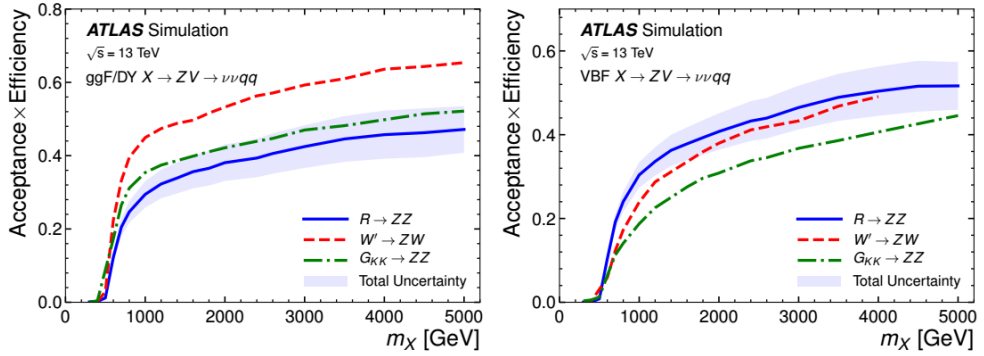

(a) (b)

Figure 6: Selection acceptance times efficiency for the $X \to ZV \to \nu\nu qq$ signal events from MC simulations as a function of the resonance mass for (a) ggF/DY and (b) VBF production, combining HP and LP signal regions. The light shaded band represents the total statistical and systematic uncertainties for the RS radion model, and the total uncertainties are similar for the other signal models.

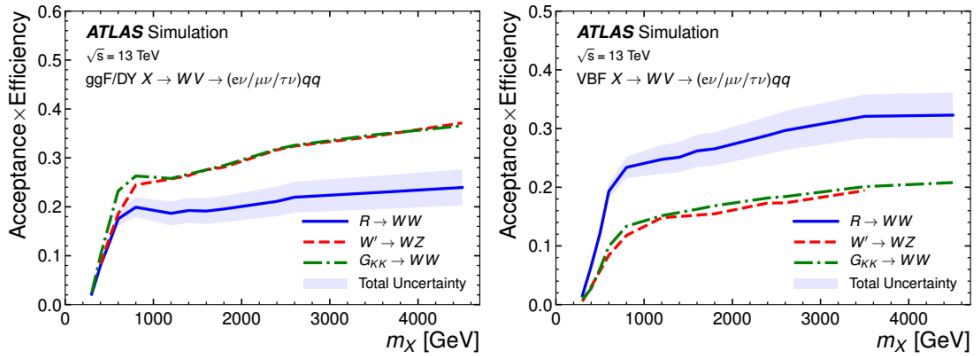

(a) (b)

Figure 7: Selection acceptance times efficiency for the $X \to WV \to (e\nu/\mu\nu/\tau\nu)\, qq$ signal events from MC simulations as a function of the resonance mass for (a) ggF/DY and (b) VBF production, combining all SRs of both the resolved and merged analyses. Signal contributions from $W \to \tau\nu$ decays are included in the acceptance calculation. The light shaded band represents the total statistical and systematic uncertainties for the RS radion model, and the total uncertainties are similar for the other signal models. The 'bump' structure around 800 GeV is due to the decreasing contribution from the resolved analysis at higher masses.

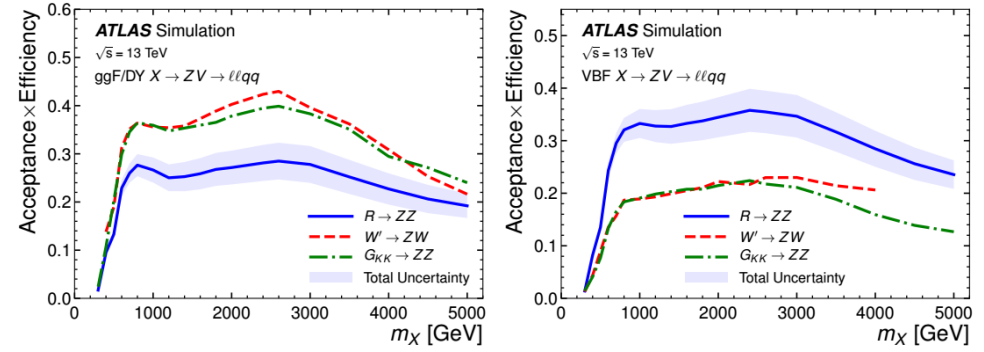

(a) (b)

Figure 8: Selection acceptance times efficiency for the $X \to ZV \to \ell\ell qq$ signal events from MC simulations as a function of the resonance mass for (a) ggF/DY and (b) VBF production, combining all SRs of both the resolved and merged analyses. The light shaded band represents the total statistical and systematic uncertainties for the RS radion model, and the total uncertainties are similar for the other signal models. The decreases in efficiencies for resonance masses above approximately 2.5 TeV are due to the merging of electrons from the highly boosted $Z \to ee$ decays. The 'bump' structure around 800 GeV is due to the decreasing contribution from the resolved analysis at higher masses.

Search for heavy diboson resonances in semileptonic final states ATLAS

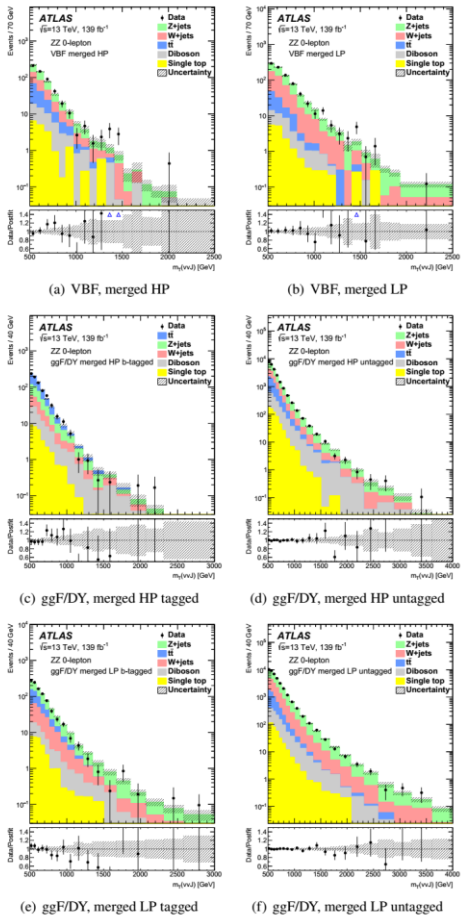

(a) VBF, merged HP (b) VBF, merged LP

(c) ggF/DY, merged HP tagged (d) ggF/DY, merged HP untagged

(e) ggF/DY, merged LP tagged (f) ggF/DY, merged LP untagged

Figure 9: Comparisons of the observed data and the expected background distributions of m_{T} in the 6 ZZ SRs of the 0-lepton channel. The background predictions are obtained through a background-only simultaneous fit to the 6 WW and 15 ZZ SRs and their respective V+jets and $t\bar{t}$ CRs (see text). The bottom panes show the ratios of the observed data to the background predictions. The blue triangles indicate bins where the ratio is non-zero and outside the vertical range of the plot. The hatched bands represent the uncertainties in the total background predictions, combining statistical and systematic contributions.

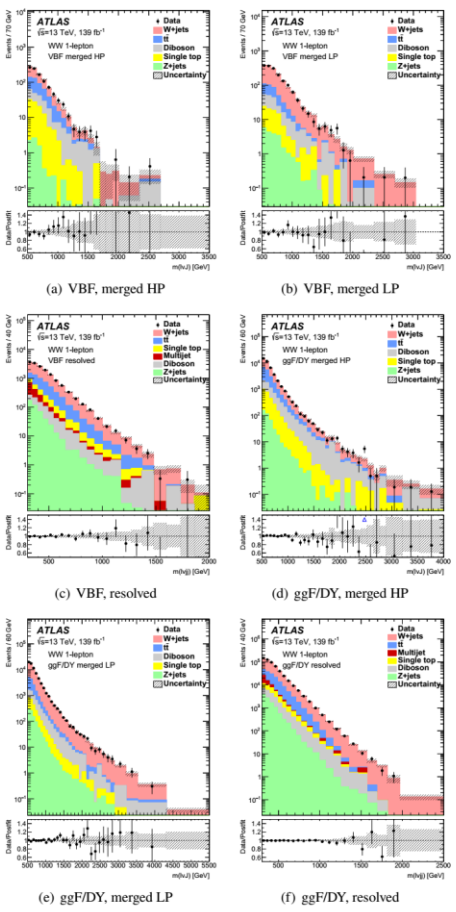

(a) VBF, merged HP (b) VBF, merged LP

(c) VBF, resolved (d) ggF/DY, merged HP

(e) ggF/DY, merged LP (f) ggF/DY, resolved

Figure 10: Comparisons of the observed data and the expected background distributions of $m_{\ell\nu jj}$ or $m_{\ell\nu J}$ in the 6 WW SRs of the 1-lepton channel. The background predictions are obtained through a background-only simultaneous fit to the 6 WW and 15 ZZ SRs and their respective V+jets and $t\bar{t}$ CRs (see text). The bottom panes show the ratios of the observed data to the background predictions. The blue triangles indicate bins where the ratio is non-zero and outside the vertical range of the plot. The hatched bands represent the uncertainties in the total background predictions, combining statistical and systematic contributions.

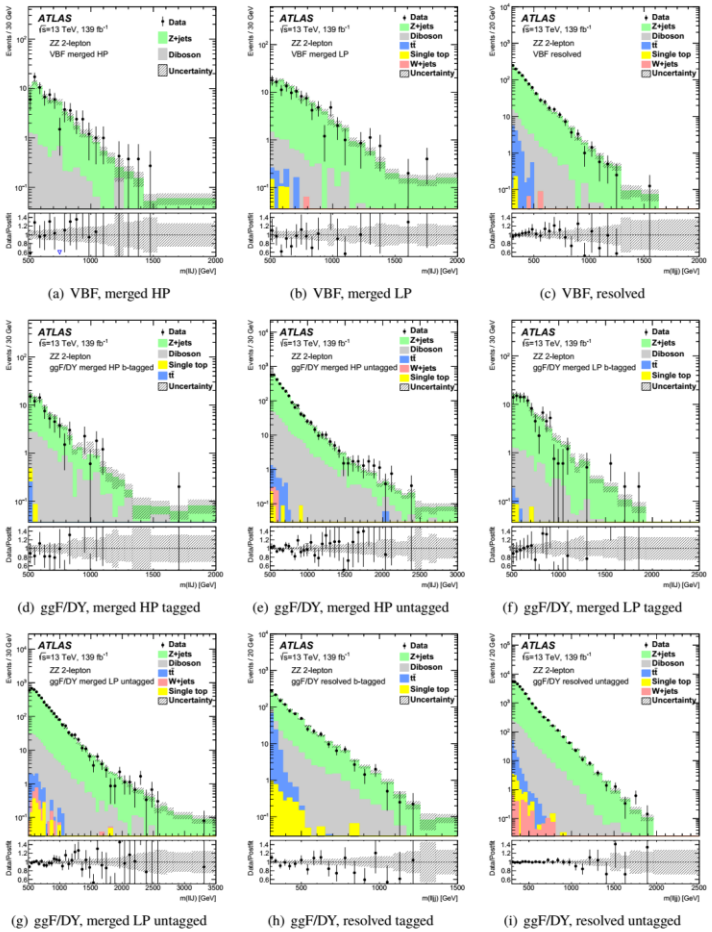

(a) VBF, merged HP (b) VBF, merged LP (c) VBF, resolved

(d) ggF/DY, merged HP tagged (e) ggF/DY, merged HP untagged (f) ggF/DY, merged LP tagged

(g) ggF/DY, merged LP untagged (h) ggF/DY, resolved tagged (i) ggF/DY, resolved untagged

Figure 11: Comparisons of the observed data and the expected background distributions of $m_{\ell\ell jj}$ or $m_{\ell\ell J}$ in the 9 ZZ SRs of the 2-lepton channel. The background predictions are obtained through a background-only simultaneous fit to the 6 WW and 15 ZZ SRs and their respective V+jets and $t\bar{t}$ CRs (see text). The bottom panes show the ratios of the observed data to the background predictions. The blue triangles indicate bins where the ratio is non-zero and outside the vertical range of the plot. The hatched bands represent the uncertainties in the total background predictions, combining statistical and systematic contributions.

Dijet resonance search with weak supervision ATLAS

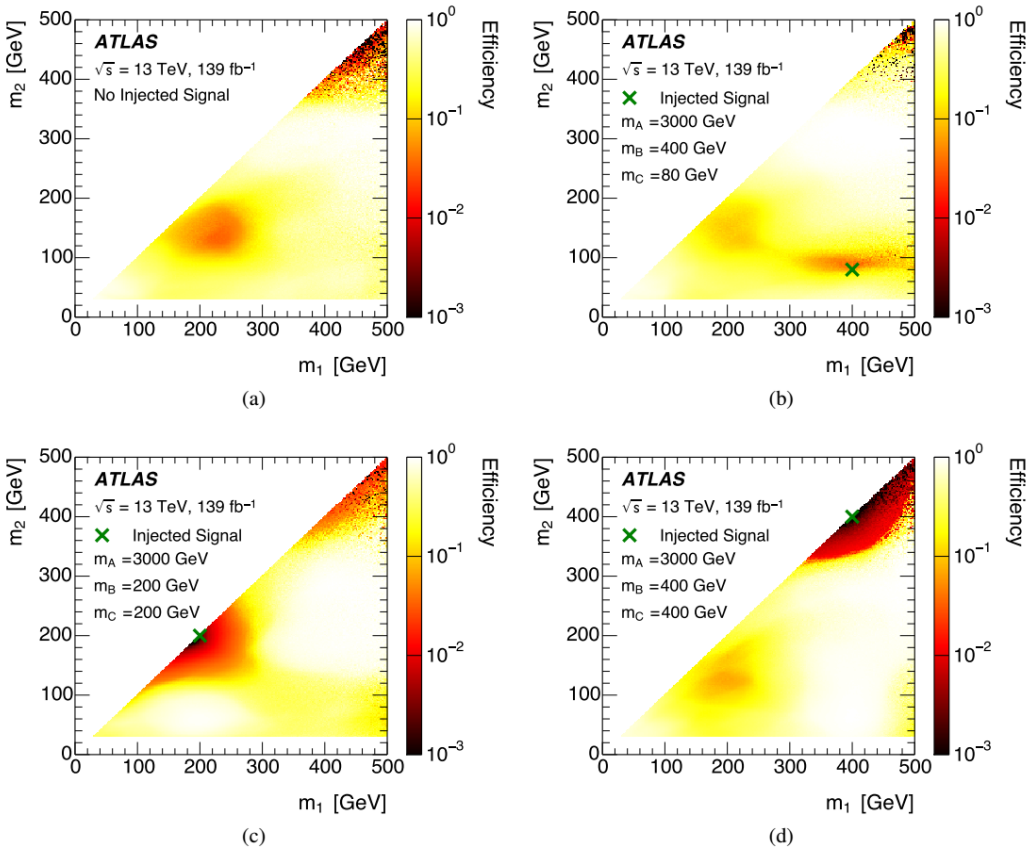

Figure 1: The efficiency mapped output of the NN versus the input variables for the events in signal region 2 for four cases: (a) there is no injected signal; (b) there is an injected signal of $m_A = 3$ TeV, and $m_B = 400$ GeV and $m_C = 80$ GeV, (c) there is an injected signal of $m_A = 3$ TeV, and $m_B = 200$ GeV and $m_C = 200$ GeV, and (d) there is an injected signal of $m_A = 3$ TeV, and $m_B = 400$ GeV and $m_C = 400$ GeV. The location of (m_B, m_C) for the given injected signal is marked with a green ×. The injected cross section is just below the limit at low m_B and m_C from the inclusive dijet search [101].

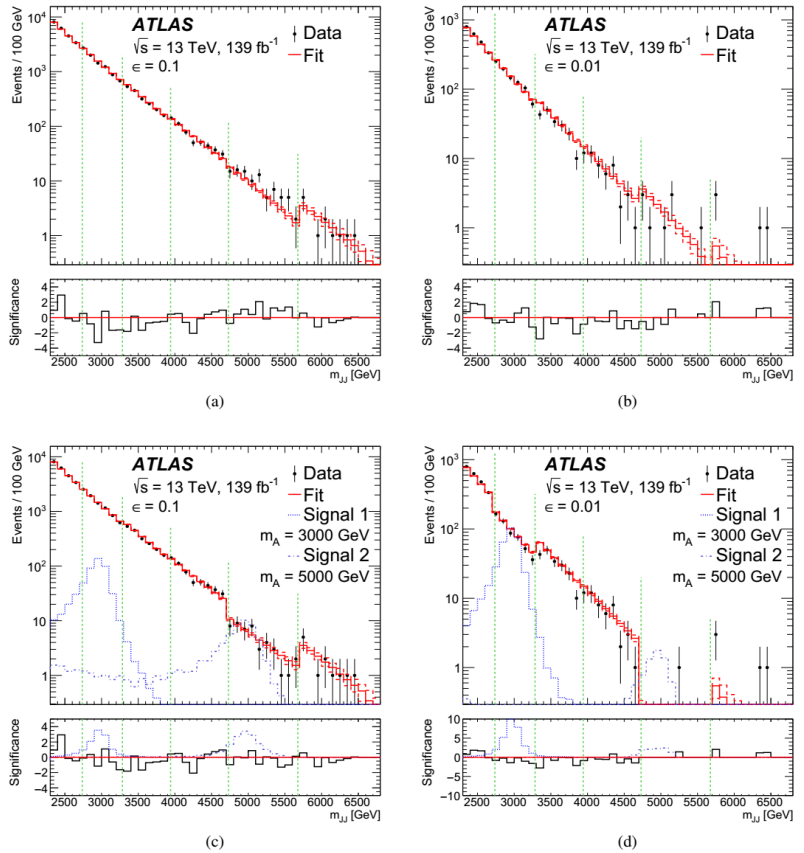

Figure 2: A comparison of the fitted background and the data in all six signal regions, indicated by vertical dashed lines, and for (a,c) $\epsilon = 0.1$ and (b,d) $\epsilon = 0.01$. Dashed histograms represent the fit uncertainty. The lower panel is the Gaussian-equivalent significance of the deviation between the fit and data. The fits are performed including the sidebands, but only the signal region predictions and observations in each region are shown. As the NN is different for each signal region, the presented spectrum is not necessarily smooth. The top plots (a,b) show the result without injected signal, and the bottom plots (c,d) present the same results but with signals injected only for the NN training at $m_A = 3$ TeV (Signal 1) and $m_A = 5$ TeV (Signal 2), each with $m_B = m_C = 200$ GeV. The injected cross section for each signal is just below the limit from the inclusive dijet search [101].

Search for large MET with one top-quark ATLAS

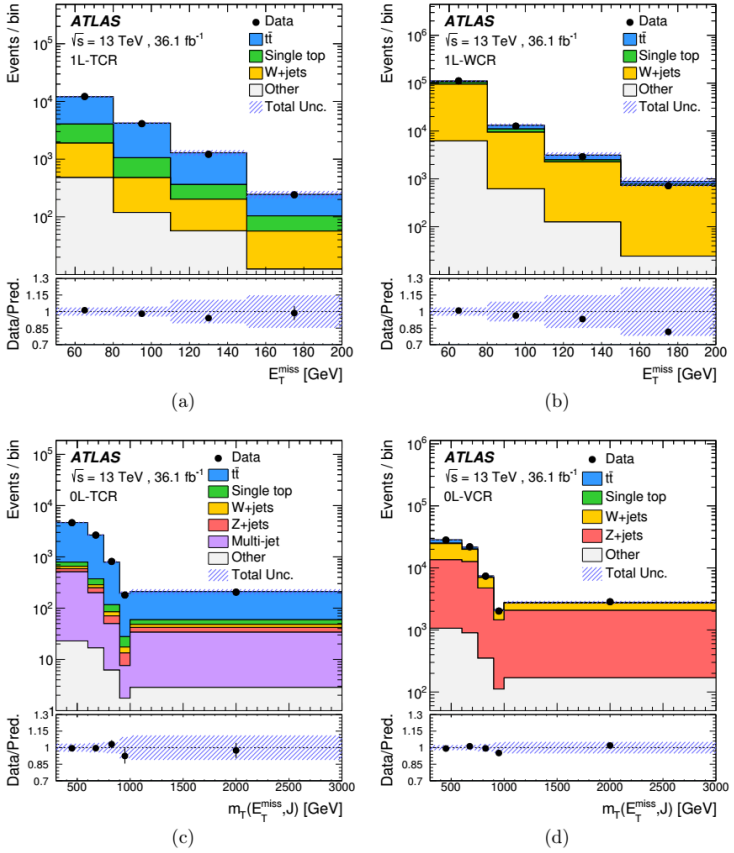

Figure 2. Comparison of data and SM prediction for the $E_{\mathrm{T}}^{\mathrm{miss}}$ distribution in (a) the $t\bar{t}$ and (b) $W+$jets control regions; and for the transverse mass of the top-tagged large-R jet and $E_{\mathrm{T}}^{\mathrm{miss}}$ system, $m_{\mathrm{T}}(E_{\mathrm{T}}^{\mathrm{miss}}, J)$, distribution in the (c) $t\bar{t}$ and (d) W/Z +jet control regions used for the dark-matter search ((a) and (b)) and vector-like T-quark search ((c) and (d)). Other backgrounds in the 1L regions include multi-jet, Z+jets and diboson contributions, while in the 0L regions it is composed of diboson, $t\bar{t}+X$ and multi-jet contributions. The expectations in the leptonic (hadronic) channel are obtained from a fit of the background-only hypothesis to data in the 1L (0L) control regions, where the normalisations of the $t\bar{t}$ and $W+$jets ($t\bar{t}$ and $W/Z+$jets) processes are treated as nuisance parameters in the fit. The error bands include statistical and systematic uncertainties. The last bin contains the overflow events.

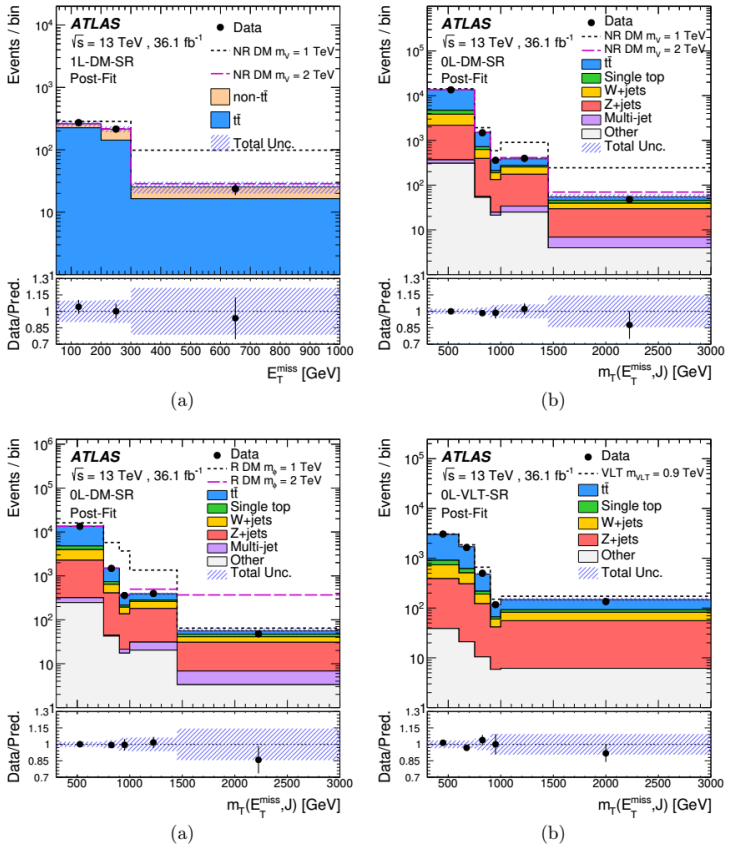

Figure 3. Comparison of data and fitted expectations for the $E_{\mathrm{T}}^{\mathrm{miss}}$ and the transverse mass of the top-tagged large-R jet and $E_{\mathrm{T}}^{\mathrm{miss}}$ system, $m_{\mathrm{T}}(E_{\mathrm{T}}^{\mathrm{miss}}, J)$, distributions in the signal regions. Other backgrounds in the 1L regions include multi-jet, Z+jets and diboson contributions, while in the 0L regions it is composed of diboson and $t\bar{t}+X$ contributions. The background-only hypothesis is used in the fit: (a) and (b) including the 1L and 0L DM signal regions as well as the 1L and 0L control regions; (c) 0L DM signal and control regions; (d) 0L VLT signal and control regions. The error bands include statistical and systematic uncertainties. The expected shape of a benchmark signal normalised to the theoretical prediction is added on top of the SM prediction. The benchmark signals correspond to: the non-resonant (NR) DM model with $m_V = 1$ TeV and 2 TeV, $m_\chi = 1$ GeV, $a = 0.5$ and $g_\chi = 1$; the resonant (R) DM model with $m_\phi = 1$ TeV and 2 TeV, $m_\chi = 10$ GeV, $\lambda = 0.2$ and $y = 0.4$; and a VLT with a mass of 0.9 TeV.

Search for single production of VLQ decaying into Wb ATLAS

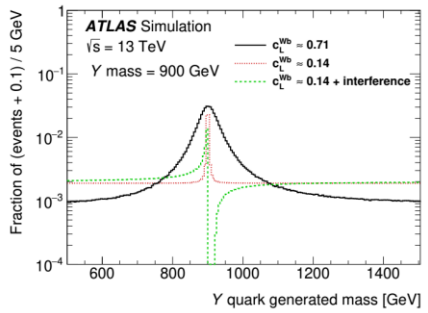

Figure 3. The generated mass distributions at particle level for a Y quark with a mass of 900 GeV, for a coupling strength of $c_0 = \kappa_T \approx 0.5$ and $c_L^{Wb} \approx 1/\sqrt{2}$ ($c_R^{Wb} = 0$, solid line) and of $c_0 = c_L^{Wb} = 0.14$ (dotted line) as defined in ref. [95]. The distribution for a right-handed only and left-handed only Y quark (solid line) is the same. The dashed line shows the generated vector-like quark mass distribution at particle level of a left-handed Y signal with a mass of 900 GeV, coupling strength of $c_L^{Wb} = 0.14$ and interference effects with the SM included. The interference effects lead to negative entries in some bins of the distribution. For better visualisation of the tail distribution including the interference effect, the bin contents of all distributions were shifted by +0.1 before normalisation.

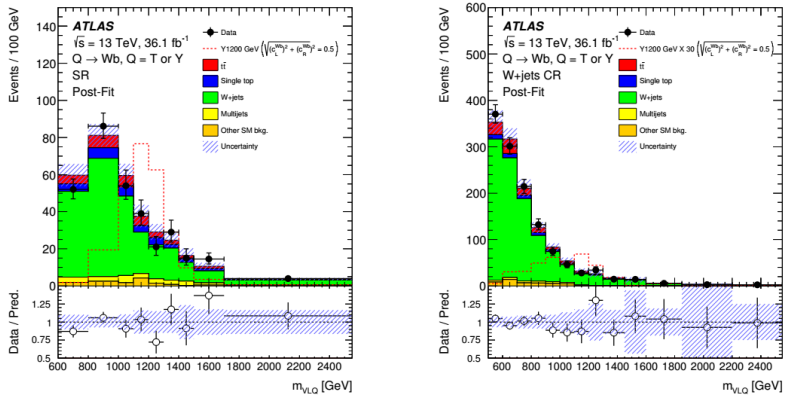

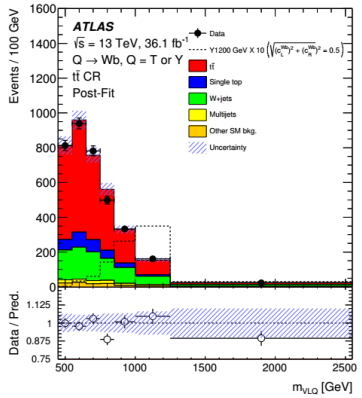

Figure 6. Distribution of the VLQ candidate mass, m_{VLQ}, in (a) the SR, (b) the W+jets CR, and (c) the $t\bar{t}$ CR, after the fit to the background-only hypothesis. The first and last bin include the underflow and overflow respectively. The lower panels show the ratios of data to the fitted background yields. The error bars represent the statistical uncertainty in the data. The band represents the total systematic uncertainty after the maximum-likelihood fit. An example distribution for a Y signal with a coupling of $\sqrt{(c_L^{Wb})^2 + (c_R^{Wb})^2} \approx 0.5$ without considering any interference effects is overlaid; for better visibility, it is multiplied by a factor of 30 in the W+jets CR and by a factor of 10 in the $t\bar{t}$ CR. While the total uncertainty decreases when performing the fit, the total uncertainty in the bins around 1450-1600 GeV and 1850-2200 GeV in (b) does not decrease due to significant statistical MC uncertainties in these two bins.

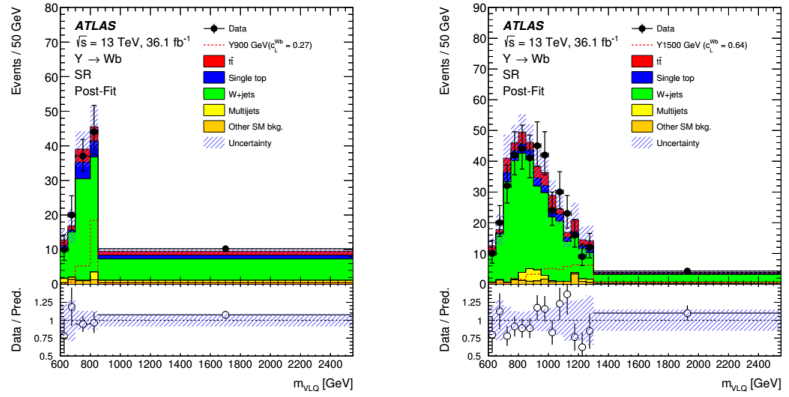

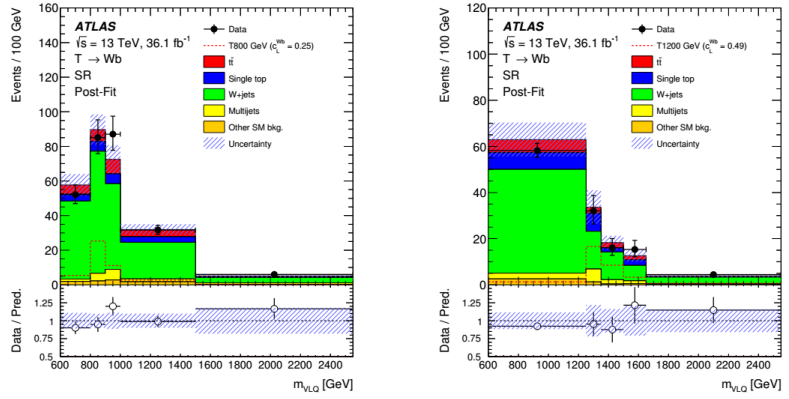

Figure 7. Distributions of the VLQ candidate mass, m_{VLQ}, after the fit to the background-only hypotheses for four different binnings chosen for four different signal masses. The first and last bin include the underflow and overflow respectively. The VLQ candidate mass distributions for (a) a left-handed Y signal with mass 900 GeV and coupling $c_L^{Wb} = 0.27$, (b) a left-handed Y signal with mass 1500 GeV and coupling $c_L^{Wb} = 0.64$, (c) a left-handed T signal with mass of 800 GeV and coupling $c_L^{Wb} = 0.25$ and (d) a left-handed T signal with mass 1200 GeV and coupling $c_L^{Wb} = 0.49$ are also shown; all signal distributions include interference. The lower panels show the ratio of data to the fitted background yields. The error bars represent the statistical uncertainty in the data. The band represents the total systematic uncertainty after the maximum-likelihood fit.

Electroweak production of vector-like T quark fully hadronic final states CMS

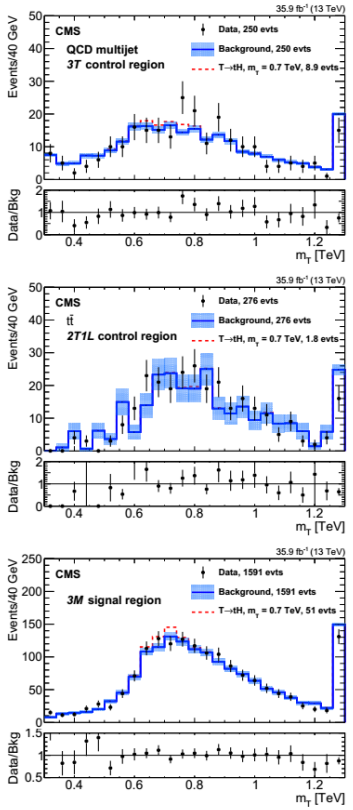

Figure 2: The five-jet invariant mass distribution (black points with error bars) for the tHbq channel after the full selection in the QCD multijet $3T$ control region (upper), the $t\bar{t}$ $2T1L$ control region (middle), and the $3M$ signal region (lower). The superimposed blue histogram, labeled "background", is the reweighted $2M1L$ region distribution, used as an estimate of the background shape, with its normalization adjusted to match the number of entries observed in each region. A potential narrow-width signal (dashed red histogram) is added on top of the blue histogram for $m_T = 0.7$ TeV and $\Gamma/m_T = 0.01$, for a product of signal cross section and branching fraction of 600 fb. The light blue shaded area corresponds to the statistical uncertainties in the corresponding $2M1L$ region. The last bin in each distribution also contains events with masses exceeding 1.3 TeV.

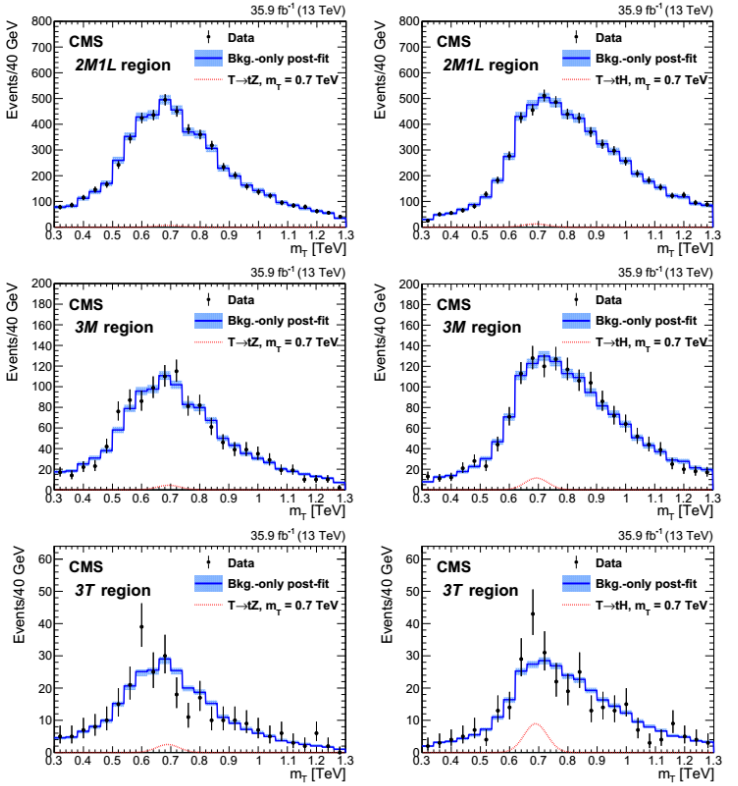

Figure 4: The background-only post-fit invariant mass distributions for the tZ candidates (left) and tH candidates (right) for each region fitted: $2M1L$ (upper row), $3M$ (middle row), and $3T$ (lower row). The signal hypothesis shown is a T with a mass of 0.7 TeV, narrow width, and a product of the cross section and branching fraction of 600 fb for the tZbq and tHbq channels. The data are represented by the black points with error bars, the signal hypothesis is represented by the red dashed line, the blue histogram gives the fitted background, and the light blue band represents the uncertainty in the background fit.

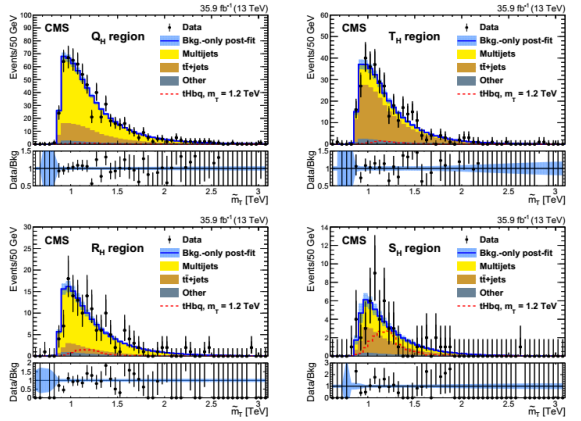

Figure 6: The background-only post-fit distributions in data for the Q_H, T_H, R_H, and S_H regions that are used as signal and control regions primarily for the T → tH channel. The upper plots show regions Q_H (left) and T_H (right), while the lower plots show regions R_H (left) and S_H (right). The dashed red histogram is an example T → tH signal for the tHbq process with a 1.2 TeVT quark mass and a fractional width of 30% with a cross section from the singlet model of 142 fb. The lower panels show the ratio of observed data to fitted background per bin. The error bars on the data represent 68% CL Poisson intervals. The light blue band in each ratio panel shows the fractional uncertainties in the fitted background.

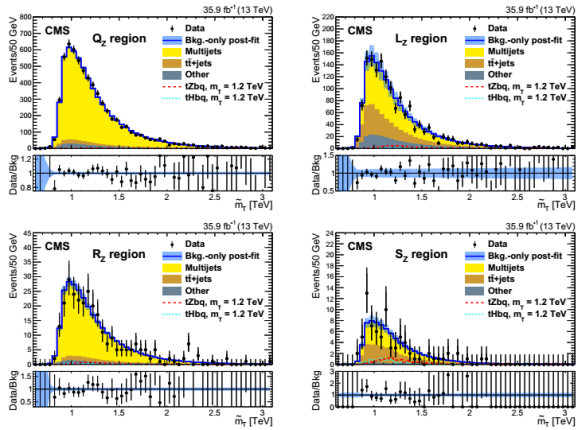

Figure 7: The background-only post-fit distributions in data for the Q_Z, L_Z, R_Z, and S_Z regions that are used as signal and control regions primarily for the T → tZ channel. The upper plots show regions Q_Z (left) and L_Z (right), while the lower plots show regions R_Z (left) and S_Z (right). The dashed red histogram is an example T → tZ signal for the tZbq process with a 1.2 TeVT quark mass and a fractional width of 30% with a cross section from the singlet model of 131 fb. The shorter dashed cyan histogram is for T → tH signal for the tHbq process with the model assumptions used in Fig. 6. The lower panels show the ratio of observed data to fitted background per bin. The error bars on the data represent 68% CL Poisson intervals. The light blue band in each ratio panel shows the fractional uncertainties in the fitted background.